INTEGRATED ROCK CLASSIFICATION IN ORGANIC-RICH MUDROCKS: A CASE STUDY ON EAGLE FORD FORMATION

A Thesis

by

SHAHIN AMIN

Submitted to the Office of Graduate and Professional Studies of
Texas A&M University
in partial fulfillment of the requirements for the degree of

MASTER OF SCIENCE

Chair of Committee,	Walter B. Ayers
Co-Chair of Committee,	Zoya Heidari
Committee Member,	Juan Carlos Laya Pereira
Head of Department,	Daniel Hill

May 2017

Major Subject: Petroleum Engineering

ABSTRACT

Formation evaluation and production design are often challenging in organic-rich mudrocks due to complexities in petrophysical and compositional properties as well as post-depositional hydrocarbon generating mechanisms such as thermal maturation over time. Petrophysical parameters such as porosity, permeability and fluid saturations are important but not sufficient to fully characterize organic-rich mudrocks. Thus, integration of geomechanical, geological, geochemical, and petrophysical characterization is critical to enhance production from these formations. This paper focuses on an integrated rock classification applied in two wells in the oil-window of the Eagle Ford Shale play in South Texas. The lower Eagle Ford interval is an organic-rich fossiliferous marine shale deposited in Late Cretaceous.

Initially, we classified the rocks based on geological texture and geochemical properties measured at the lower Eagle Ford (LEF) in a well where conventional core was available. Then, I performed a joint inversion of triple-combo, spectral gamma ray, and elemental capture spectroscopy (ECS) logs in both wells to estimate depth-by-depth volumetric concentrations of minerals, porosity, and fluid saturations. The rocks were separated into five petrophysical classes using these results. In the absence of acoustic measurements in Well 1, I used concentrations and shape (i.e., aspect ratio) of minerals as inputs to the Self-consistent Approximation (SCA) model to estimate depth-by-depth effective elastic properties such as Young's Modulus (YM), Poisson’s Ratio (PR), and minimum horizontal stress (MHS) gradient. Finally, I conducted a geomechanical

classification, and divided the rocks in the LEF into three categories: low-stress, medium-stress and high-stress, based on the MHS gradient.

The introduced well-log-based petrophysical and geomechanical rock classification was applied to the pilot section of two oil-producing wells located approximately 20 miles apart. Both wells were drilled horizontally with lateral lengths greater than 5,000 ft, and were hydraulically fractured. Petrophysical evaluation showed similar organic content (4.5- 5.0 wt%), porosity (7.0%), and total volumetric concentration of clays (10-15 vol%) in the target intervals of both wells. However, in comparison of well productivity, Well 1 produced an additional 11,000 barrels of oil equivalent (BOE) with a total hydrocarbon production of 54,000 BOE in the first 90 days after completions, approximately 25% more than Well 2 (43,000 BOE total). Geomechanical rock classification results showed lower MHS average values in Well 1, than in Well 2 (0.58 psi/ft vs. 0.62 psi/ft, respectively), and a higher proportion of completion-quality (low-stress) rock types in Well 1 relative to Well 2 (55% vs. 34% respective).

Results suggest that the well-by-well difference in production cannot be explained by only relying on the estimated petrophysical properties of the formation. Higher productivity of Well 1 may result from greater hydraulic fracture extent, and thus increased total stimulated reservoir volume (SRV). Moreover, geomechanical properties such as in-situ stresses and presence of natural fractures play important roles towards well productivity and must be taken into account in rock classification for completion decisions.

DEDICATION

This thesis is dedicated to my parents and younger sister, for their unconditional love, courage, and support throughout my life.

ACKNOWLEDGEMENTS

I would like to thank my family and friends for their inspiration and endless support, which motivated me to continue my education towards obtaining my Master of Science degree.

CONTRIBUTORS AND FUNDING SOURCES

Contributors

I would like to express my sincere gratitude to my advisor, Dr. Zoya Heidari, for her vast knowledge, patience, and motivation throughout my undergraduate and graduate research efforts. In addition, I would like to thank Dr. Walter Ayers and Dr. Juan Carlos Laya for serving as my committee members, as well as for their positive feedback on this research.

Special thanks to Matthew Wehner and Dr. Michael Tice from Halbouty Department of Geology and Geophysics at Texas A&M University for their technical advice on the geological aspect of this project.

I appreciate the Department of Petroleum Engineering and the Department of Geology and Geophysics at Texas A&M University for providing core and well-log measurements used in my research. I also appreciate Andrew Russell from W.D. Von Gonten Laboratories for conducting X-ray diffraction measurements for this project.

Funding Sources

Research reported in this thesis was generously funded by the Joint Industry Research Program on "Multi-Scale Formation Evaluation of Unconventional and Carbonate Reservoirs" at Texas A&M University, jointly sponsored by Aramco Services Company, BHP Billiton, BP, Chevron, ConocoPhillips, and Devon Energy.

NOMENCLATURE

α	Geometric grain shape factor
α_{b}	Biot's constant
E	Young's modulus, GPa
σ_{hmin}	Minimum horizontal stress, GPaOverburden stress, GPa
σ_v	Overburden stress, GPa
K	Bulk modulus, GPa
K_m	Bulk modulus of the mineral phase (zero-porosity), GPa
Q^{*i}	Shape coefficient of an inclusion in self-consistent approximation model
S_1	Free hydrocarbon content measured in rock pyrolysis test, weight fraction
S_w	Water saturation, fraction
μ	Shear modulus, GPa
N	Number of components in self-consistent approximation model
P^{*i}	Shape coefficient of an inclusion in self-consistent approximation model
P_p	Pore pressure, GPa
T_{max}	Temperature at S_2 peak in pyrolysis, celcius
v	Poisson's ratio
V_{clay}	Total clay volume, fraction
x_i	Volumetric concentration of component *i* in self-consistent approximation model

2D	Two-dimensional
BBL	Barrel
BCF	Billions of Cubic Feet
BOE	Barrel of Oil Equivalent
ECS	Elemental Capture Spectroscopy
EIA	Energy Information Administration
GOR	Gas-oil-ratio
GPa	Giga Pascal, 1GPa=1E9 Pa
HI	Hydrogen Index
LEF	Lower Eagle Ford
MHS	Minimum Horizontal Stress
PCA	Principal Component Analysis
PR	Poisson's Ratio
PRC	Petrophysical Rock Classification/Class
PSI	Pounds per Square Inch
RC	Rock Class
SCA	Self-consistent Approximation
SPRC	Stress-Profiles Rock Classification/Class
SRV	Stimulated Reservoir Volume
TOC	Total Organic Carbon
UEF	Upper Eagle Ford
XRD	X-ray Diffraction

XRF	X-ray Fluorescence
YM	Young’s Modulus

TABLE OF CONTENTS

Page

LIST OF FIGURES

Page

LIST OF TABLES

Page

1. INTRODUCTION*

Geoscientists have introduced different techniques to classify sedimentary rocks based on their mineralogy and properties. Each rock classification method utilizes specific data depending on the purpose of the classification. In the case of organic-rich mudrocks, integrated classification schemes that take into account petrophysical, compositional, and geomechanical properties greatly improve rock characterization and formation evaluation. In this section, I briefly summarize the previously published literature on rock classification, state the problems and challenges, and finally list the research objectives pursued in this thesis.

1.1 Literature Review

Among the first geological rock classification studies, in the early 1900's, Grabau (1904) divided sedimentary rocks based on their origin and forming mechanisms, into two main groups: endogenetic and exogenetic. Non-clastic rocks that are not composed of fragments of older rocks were chemically deposited and belong to the endogenetic rock class. On the other hand, clastic rocks composed of fragments of older rocks were formed mainly through mechanical processes and belong to the exogenetic rock class in Grabau's classification. Decades later, an increase in acquisition of core and well-logs as well as advances in visual aids lead to improved rock

*Parts of the introduction and research objectives sections presented in this chapter have been reprinted from "Rock Classification in the Eagle Ford Shale through Integration of Petrophysical, Geological, and Geochemical Characterization" by Shahin Amin, Matthew Wehner, Zoya Heidari, and Michael Tice. SPWLA-2016-KKK.

characterization and subsequently more reliable rock classification. In a petrophysical rock classification scheme, Archie (1952) classified carbonates into three categories: compact crystalline, chalky, and sucrose. Texture of the matrix and characteristics of the visible pore structure were the basis of this classification. Archie's porosity-based classification differentiated limestones based on petrophysical properties for selection of reservoir quality rocks. Increase in availability and use of thin-section images, particularly for interpretation of depositional environments, shaped the texture-based geological rock classification schemes. Classification based on depositional texture was found to be a helpful adjunct to other classifications such as mineralogical classifications. Folk (1962) introduced a detailed texturally-based classification that incorporated grain size, roundness, sorting and packing, as well as grain composition using microscopic images. In a similar approach, Dunham (1962) classified carbonate rocks based on the ratio of grain to matrix into two main groups: grain-supported and mud-supported. In this classification, the term "mud" refers to grains smaller than 20 microns in size, contrasting with "grain" particles that are larger than 20 microns.

Subdivisions to Dunham's classification are based on the percentage of grains in texture. Mud-supported carbonates are the most common where the grains are not abundant enough to support one another ("floating" grains). These rocks are classified as "mudstone" when they contain less than 10% grains and "wackestone" when more than 10% grains are present. On the other hand, rocks where the grains are abundant enough to support one another fall under the grain-supported category, with further subdivisions

based on presence of mud (particles of clay and fine silt size). When the rock is grain-supported and lacks mud it is called "grainstone," and it is called "packstone" if mud is present. As of today, the original and modified versions of Dunham's carbonate classification are still being used by geologists to interpret depositional environments.

In the past few decades, more quantitative core- or well-log-based rock classifications were introduced and applied to a variety of unconventional reservoirs such as tight sandstone/carbonate and organic-rich formations. Due to complexities in composition and pore structure of these rocks, integration of different data types is used commonly for a more reliable rock characterization. For instance, integration of geochemical data (i.e., X-ray fluorescence or ECS logs) with core mineral concentration measurements such as X-ray diffraction (XRD) enables accurate quantitative mineral modeling, leading to a reliable estimation of petrophysical and compositional properties. Improvement of the results is achieved with the use of statistical element-mineral or mineral-mineral relationships in the petrophysical model (Quirein et al., 2010). Geochemical measurements can be conducted both at the laboratory and the wellsite, and are applicable as an evaluation technique in organic-rich mudrocks.

Rushing et al. (2008) conducted an integrated core-based rock typing in the Bossier tight sand formation. A total of 1,000 ft of whole core was extracted for both qualitative and quantitative analysis from three wells. The three different rock classification methods applied to this formation were depositional, petrographic and hydraulic. Depositional rock classes were identified by geological core description based

on existing Bossier sand depositional models in order to provide information on texture, sedimentary structures, and stratigraphic sequences. For petrographic rock classification, microscopic images at pore scale and X-ray diffraction data were analyzed to describe the current pore structure, texture, composition, and clay type distributions. Furthermore, quantitative measurements of porosity and permeability, as well as mercury injection capillary pressure measurements were utilized to classify the formation rocks into five hydraulic rock classes. Pore throat radius, calculated from the capillary pressure measurements, was used as the main parameter to determine the reservoir quality in hydraulic rock classes. Integration of the results showed that due to the significant post-depositional diagenesis and the alteration in physical properties of the rocks, the depositional rock classes were not good indicators of reservoir quality in this formation. While petrographic rock classes showed a slightly better correlation with porosity-permeability relationships, still no strong or unique relationships were observed. However, the integration of detailed geological description with petrophysical properties improved rock characterization in the Bossier tight sand formation.

Kale et al. (2010) conducted a core-based rock classification in the Barnett shale. 800 core plugs covering 1,600 ft were extracted from four wells. Measurements of porosity, total organic carbon (TOC), mineralogy, and capillary pressures were obtained from these cores. Three “petrofacies” were identified based on the core measurements and the previous Barnett lithofacies classifications, showing distinct capillary pressure curves and microstructure determined by environmental scanning electron microscope

(ESEM). Further, principal component and cluster analysis on petrophysical and compositional parameters was conducted on the same data set. Although the output rock classes based on cluster analysis were not as distinct as the petrofacies classification, similar ranges in measured parameters were observed between the two methods. The result of the described rock classification was compared in the perforated zones of two wells ('A' and 'B') with different gas production. Percentage of the highest quality rock class in the perforated interval of well 'A' was significantly higher than well 'B', resulting in a 40% higher gas production.

In a well-log-based study, Popielski et al. (2012) conducted a classification using "k-means" clustering and factor analysis (i.e., used in reduction of the dimension of input data) to group rocks with similar well-log responses and well-log derived estimates. A synthetic case was used to compare the results between two cases: (a) the conventional well-logs were used as the inputs to the rock classification, and (b) an inverted version of the well-logs were used as the inputs to the rock classification. In cases where bed thickness was smaller than sampling interval, classification using inverted well-logs was more reliable, partially avoiding shoulder bed effects. Field application of the rock classification using inverted log properties in Barnett shale showed 40% increase in organic-rich rock class compared to the classification based on conventional well-logs (density, neutron, photo electric factor, and resistivity). Furthermore, Petriello et al. (2013) introduced a well-log-based multivariate classification that employed the Heterogeneous Rock Analysis (HRA) algorithm. Similar

rock patterns were identified and grouped along the zone of interest. Petrophysical and geochemical measurements were conducted on more than 200 core samples, where gas-filled porosity, pressure decay permeability, and TOC were the discriminant factors between rock classes in the Haynesville shale.

In the case of organic-rich mudrocks, interpretation of inorganic geochemical data has been used in determination of mineralogy, clay types, and modeling total organic carbon. Moreover, trace element enrichment in the rocks provides insights on paleoproductivity and paleoredox conditions at the site of deposition of organic-rich mudrocks (Wright and Ratcliffe, 2010). Redox-sensitive trace metals, which are less soluble under reducing conditions, are enriched in oxygen depleted sedimentary facies. However, some trace elements require both reducing conditions and organic matter to accumulate appreciably in shales. Elements such as molybdenum (Mo), vanadium (V), and uranium (U) provide information about redox state at the water column during deposition and also quality of organic matter/hydrocarbons (Tribovillard et al., 2006; Brumsack, 2006; Lewan, 1984). Driskill et al. (2012) conducted an integrated chemostratigraphic rock classification in the Eagle Ford formation using mainly elemental ratios of major and trace elements to generate depositional cycles and stratigraphic mapping around the basin.

Production of hydrocarbons from organic-rich mudrocks is not only dependent on the petrophysical properties. To maximize wellbore-reservoir contact, and create high permeability pathways for hydrocarbon flow, practices such as horizontal drilling, and

hydraulic fracturing are widely used in the industry. Hence, geomechanical evaluation in organic-rich mudrocks is required to model fracture geometry before planning well completions to improve the effectiveness of these operations. In a well-log-based rock classification approach that accounted for elastic properties, Saneifar et al. (2014) included a brittleness index as an additional factor of rock quality to organic-richness, kerogen porosity, and quartz and illite volumes. This integrated study used a predetermined number of geological facies in Haynesville Shale as an input to the classification. The results of the classification were then cross-validated with the thin-section petrography images for each class. Aderibigbe et al. (2016) incorporated stress profiles in a production-oriented rock classification, applied to the Wolfcamp formation. The completion intervals were selected based on the final results of the integrated rock classification.

Previous publications have demonstrated the significant impact of reliable rock classification on enhancement of formation evaluation, and subsequently an improved selection of completion intervals (Suarez-Rivera et al., 2011; Petriello et al., 2013; Aderibigbe et al., 2016). Reliability of rock classification can be assessed depending on the input parameters and its application (e.g., reserve- or production-oriented classification).

1.2 Statement of Problem

Past rock classification studies used various methods and data types as inputs to the classification. Depending on the purpose of the classification and availability of data, these inputs could be core measurements, well-logs, or well-log-based estimates of rock properties. However, core-based classifications often require a large number of measurements at a higher cost than well logs and are not practical for field-wide applications. Therefore, well-log-based classifications are favored in the industry because they provide complete vertical coverage, have greater availability of data at all wells, and cost less.

To develop a reliable well-log-based classification, proper selection of the input factors, determination of an accurate number of rock classes, and a reliable depth-by-depth assessment of petrophysical, compositional and geomechanical properties is required.

For organic-rich mudrocks, reliable classification should take into account properties such as storage capacity, fluid saturations, mineralogy, and quantity and type of organic matter as input factors to fully characterize these rocks. The majority of the past rock classifications accounted only for a fraction of these properties as inputs to the classification. Furthermore, geomechanical evaluation in organic-rich mudrocks is required to assess the effectiveness of practices such as horizontal drilling and hydraulic fracturing. These practices are widely used in the industry to maximize wellbore-reservoir contact and create high permeability pathways for hydrocarbon flow.

Previously introduced rock classification methods often did not incorporate elastic properties as an input parameter.

In the absence of sufficient core data, statistical methods have been used in some cases to identify the number of clusters in a multi-dimensional space. However, when distinct natural clusters are not present, these methods produce unreliable results. Therefore, an adequate geological knowledge of the formation rock facies is preferred in order to determine the number of output rock classes in a well-log-based rock classification design. To identify geological facies in a formation, integration of core images and measurements is recommended. Well-log based estimation of petrophysical and compositional properties can also be improved by incorporation of element-mineral or mineral-mineral relationships obtained from this integration.

A reliable well-log-based rock classification that assimilates petrophysical, compositional and geomechanical properties of the rocks can resemble the geological facies in the formation. Integration of geochemical and petrophysical data results in reduction of uncertainties in well-log-based estimates of rock properties. Moreover, inclusion of elastic properties in the rock classification enables a comprehensive characterization of organic-rich mudrocks.

Advantages of well-log-based classifications are: (a) they are more practical in the field due to lower costs and lower time associated with well-log data acquisition, and (b) they enable complete vertical coverage in the well. Application of the introduced

well-log based rock classification in the field can enhance the selection of completion zones and well-to-well comparison for hydrocarbon production potential.

1.3 Research Objectives

Integration of geological, geochemical, petrophysical, and geomechanical data is required for conducting a reliable well-log-based rock classification that fully characterizes organic-rich mudrocks. Application of an integrated rock classification in the field can improve completion design and consequently production performance in new wells where only well-logs are available. The main objectives of this research are to:

i. Conduct a core-based geological classification using whole core and thin-section images of the lower Eagle Ford formation in Well 1.
ii. Conduct a geochemical classification based on depth-by-depth X-ray fluorescence (XRF) and TOC measurements in Well 1.
iii. Conduct a well-log-based petrophysical classification based on estimates of porosity, fluid saturations, and volumetric concentration of clays in Wells 1 and 2.
iv. Conduct a well-log-based geomechanical classification based on the estimated rock stress-profiles in Wells 1 and 2.
v. Identify and characterize reservoir quality rock classes through an integrated analysis of petrophysical, geochemical, geological classification results.

vi. Recommend the best candidate rock types for well completions through integration of geomechanical, geological, geochemical and petrophysical classifications.

vii. Investigate possible reasons for the difference in well productivity using an integrated analysis of the results.

The following sections include the methods employed for geological, geochemical, petrophysical, and geomechanical classifications, as well as the results obtained in the lower Eagle Ford formation.

2. METHODS*

This section includes the step-by-step procedures conducted to obtain geochemical, geological, petrophysical, and geomechanical classifications in the lower Eagle Ford formation. I start with well-log-based petrophysical evaluation of the formation followed by a depth-by-depth assessment of geomechanical parameters, including the assessment of elastic properties and estimation of minimum horizontal stress gradients. Next, I describe the methods used for geochemical, geological, petrophysical, and geomechanical classification techniques. To identify the reservoir quality rock classes, I integrate the results of the petrophysical, geological, and geochemical rock classifications. To recommend target intervals for lateral well placement and improve hydraulic fracture design, I integrate the results of the geomechanical classification with the petrophysical, geological, and geochemical classifications. Finally, I apply both well-log-based rock classification methods to a new test well with a different hydrocarbon production to recommend best candidate zones for completions, and investigate possible factors affecting the well performance. Additionally, in the assessment of well productivity, I conduct a comparison based on stress profile distribution among the wells included in this thesis.

*Parts of the methods section presented in this chapter have been reprinted from "Rock Classification in the Eagle Ford Shale through Integration of Petrophysical, Geological, and Geochemical Characterization" by Shahin Amin, Matthew Wehner, Zoya Heidari, and Michael Tice. SPWLA-2016-KKK. Copyright 2016 by the Society of Petrophysicists and Well-Log Analysts. Reproduced with permission of SPWLA. Further reproduction prohibited without permission.

2.1 Well-log-based Petrophysical Evaluation

I determine Lower Eagle Ford boundaries based on responses of gamma ray, and uranium concentration from spectral gamma ray logs. A significant increase in total gamma ray and uranium content indicates a transition from upper to lower Eagle Ford. Additionally, a unique pyrite-rich marker bed indicates the transition to lower Eagle Ford from the top (Lock et al, 2011). In the bottom of the lower Eagle Ford, the boundary with Buda limestone is well-known due to the changes in basic well-log responses such as gamma-ray, neutron porosity, and density logs. Total organic carbon content (TOC) is estimated using a correlation obtained between TOC (wt%) from core measurements and bulk density from well logs. Assuming a constant kerogen density, depth-by-depth volumetric concentration of kerogen is then estimated. The estimates for volumetric concentration of kerogen are inputs to the inversion-based multi-mineral analysis workflow.

I jointly interpret triple-combo and ECS logs to estimate depth-by-depth mineral concentrations and petrophysical properties such as porosity and fluid saturations. In this process, determination of the mineral types is based on X-ray diffraction (XRD) measurements, average of one sample per 15 feet (5 m), in the lower Eagle Ford interval. Furthermore, I use correlations of element-to-mineral and mineral-to-mineral as additional constraints in the multi-mineral analysis to decrease non-uniqueness of the inversion results and to improve the reliability of the estimated properties. Finally, I compare the well-log-based estimates of mineral concentrations against core XRD

measurements to validate the reliability of the multi-mineral model. I estimate water saturation in the lower Eagle Ford using the modified Simandoux model (Bardon and Pied, 1969). The constant parameters in the model are obtained through calibration against core measurements. The same constant parameters are used for water saturation assessment in wells where core data is not available.

2.2 Depth-by-depth Assessment of Geomechanical Properties

In the absence of acoustic logs, I apply the self-consistent approximation (SCA) model to calculate depth-by-depth elastic properties such as bulk and shear moduli. SCA theorem assumes that the constituents of the mixture are immiscible, in an isotropic elastic media. The inputs to the SCA equations are (a) volumetric concentration of each constituent, (a) elastic moduli specific to each component, and (c) the geometric shape factor associates with that component (Berryman, 1995). SCA equations to solve for composite bulk and shear moduli are described by

$$\sum_{i=1}^{N} x_i \left(K_i - K_{SC}^{*} \right) P^{*i} = 0 \tag{1}$$

and

$$\sum_{i=1}^{N} x_i \left(\mu_i - \mu_{SC}^{*} \right) Q^{*i} = 0 \tag{2}$$

where x_i is the volumetric concentration of component i, N is the total number of constituents, K^*_{SC} and μ^*_{SC} are the bulk and shear moduli of the host rock, K_i and μ_i are

the bulk and shear moduli of the component *i*. P^*_i and Q^*_i are factors dependent of the shape assigned to each constituent. I assign shape factors for each component based on the analysis of two-dimensional (2D) X-ray elemental distribution maps. Finally, Young's Modulus (YM or *E*) and Poisson's Ratio (PR or *v*) are calculated via

$$E = \frac{9K^*_{SC}\mu^*_{SC}}{3K^*_{SC} + \mu^*_{SC}} \tag{3}$$

and

$$v = \frac{3K^*_{SC} - 2\mu^*_{SC}}{2\left(3K^*_{SC} + \mu^*_{SC}\right)} \tag{4}$$

Furthermore, to plan well completions design and hydraulic fracture design, I estimate depth-by-depth minimum horizontal stress (MHS) gradient via

$$\sigma_{h\min} = \frac{\nu}{1-\nu}(\sigma_v - \alpha_b P_p) + \alpha_b P_p \tag{5}$$

where σ_h is the minimum horizontal stress, σ_v is the overburden stress, P_p is the pore pressure, *v* is the Poisson's Ratio, and α_b is the Biot's constant. Bulk density and resistivity logs were used to predict the overburden stress and pore pressure in this case. I estimate Biot's constant at each depth via

$$\alpha_b = 1 - \frac{K}{K_m} \tag{6}$$

where *K* is the bulk modulus of the rock including both mineral and fluid phases, and K_m is the zero-porosity (i.e., only mineral phase) bulk modulus. The bulk and shear moduli

are estimated using the SCA method (**Equation 1** and **Equation 2**).

2.3 Geological Rock Classification

Variation in depositional environment moving upward from the base of Eagle Ford is noticeable in the texture of the extracted cores. I identify these differences in texture based on full core photos in addition to thin-section images. The names assigned to the lithofacies are based on (a) the ratio of grain to matrix (percentages of fossils in the matrix) according to Dunham's carbonate classification (b) degree of lamination, and (c) type of the existing fossils.

2.4 Geochemical Rock Classification

To classify rocks based on inorganic geochemical data, I use depth-by-depth core X-ray fluorescence (XRF) measurements in the lower Eagle Ford formation. Through the analysis of major and trace element concentrations, I divide the formation into chemostratigraphic units. The geochemical classification explains vertical variations in paleo productivity and redox conditions in depositional environments, and post depositional processes such as diagenesis, organic maturation, and hydrocarbon generation. Finally, I conduct a class-by-class analysis of parameters such as hydrogen index, oxygen index, and thermal maturity, based on Rock-Eval Pyrolysis core measurements.

2.5 Petrophysical Rock Classification

After depth-by-depth estimation of petrophysical, compositional, and geomechanical properties, I conduct a well-log-based rock classification, adopting a hierarchical clustering algorithm to group similar rocks by minimizing the total intra-class variance in each step (Ward, 1963). I assign the input number of rock classes based on the total number of geological facies obtained from the combination of core and geochemical evaluations.

2.6 Geomechanical Rock Classification

I classify rocks in the lower Eagle Ford formation to low-, medium-, and high-stress, based on the well-log-based estimates of minimum horizontal stress (MHS) at each measured depth. The results of the geomechanical rock classification illustrates the vertical distribution of rocks with different levels of minimum horizontal stress in the pilot section of the wells included in this paper.

3. FIELD EXAMPLE: EAGLE FORD FORMATION*

I applied the described method to the Lower Eagle Ford formation. This section includes an overview on the geology of the Eagle Ford formation and the results of the described rock classification schemes in two wells (Wells 1 and 2) located in the oil window of the Eagle Ford formation.

3.1 Geological Background of the Eagle Ford Formation

Eagle Ford formation, located in Texas, is the biggest North American shale play in terms of liquid hydrocarbon production, peaking approximately 1.6 million barrels of oil equivalent per day (MMBOE/d) accompanied by 5 billions of cubic feet per day (BCF/d) of natural gas production in 2015 (U.S. Energy Information Administration (EIA) , 2015). Petrohawk drilled the Eagle Ford discovery well in LaSalle County in 2008, with initial of natural gas flow of 7.6 MMCF/d. Since then, over 20,000 Eagle Ford drilling permits were issued in Texas, with substantial increase in production every year (Texas Railroad Commission, 2015).

*Parts of the results section presented in this chapter have been reprinted from "Rock Classification in the Eagle Ford Shale through Integration of Petrophysical, Geological, and Geochemical Characterization" by Shahin Amin, Matthew Wehner, Zoya Heidari, and Michael Tice. SPWLA-2016-KKK. Copyright 2016 by the Society of Petrophysicists and Well-Log Analysts. Reproduced with permission of SPWLA. Further reproduction prohibited without permission.

During the Jurassic and Cretaceous periods in the northwest part of the Gulf of Mexico, the paleotopography was related to the evolution of the Comanche Reef Platform as it grew and eroded based on relative sea level. The deposition of the Eagle Ford sediments was on a carbonate platform that had uneven topography due to erosion (Faust, 1990; Donovan and Staerker, 2010). Thus, when the platform began to be flooded, sometime from early to middle Cenomanian at the beginning of the Late Cretaceous, the basins experienced restriction and episodic anoxia. There is evidence that the event depositions in the Eagle Ford Group not only included ash bed falls but also storm deposits. The Eagle Ford sediments primarily consists of alternating mudstone/marlstones with limestones along with varying levels of organic content (up to 10 wt% TOC), and occasional bentonitic ash beds. The Lower Eagle Ford Formation (which in the subsurface contains the unconventional reservoir) appears to have been deposited during basin restriction, storm deposition and episodic anoxia; these factors likely contributed to the ultimate incorporation of organic matter (Wehner et al., 2015). These conditions make the Eagle Ford Formation highly heterogeneous in the vertical dimension. Some of this vertical heterogeneity can be predicted by sequence stratigraphy (Donovan and Staerker, 2010; Donovan et al., 2012; Donovan et al., 2013). Gardner et al., (2013) investigated the lateral variation of Eagle Ford Group sediments and noted a difference depending on whether upper or lower part of the Eagle Ford Group was considered. However, the variation is minor at scales up to 3 mi (5 km), unlike the vertical variation. Factors that influence vertical variation include sea-level at time of

deposition, sediment source, organic productivity, storm frequency, and dominant diagenetic mechanisms.

The Eagle Ford Shale sequence overlies Buda limestone, and is overlain by the Austin Chalk. Depositional sequences of Eagle Ford are a transgressive lower member, and a highstand upper member. The unconventional reservoir associated with organic-rich mudstones is in the lower part of Eagle Ford. From the Maverick Basin in South Texas to the San Marcos Arch in Central Texas, the upper section of Eagle Ford is truncated beneath the unconformity at the top of Eagle Ford (Donovan and Staerker, 2010). Lower Eagle Ford is characterized by high organic content, and can be distinguished by increase in Uranium content from spectral gamma ray logs (ranging from 5-15 ppm in LEF section). Thin-section image analysis is conducted in to describe the depositional texture of the rocks based on the observed mineralogy and features. Dunham's (1962) carbonate classification scheme is commonly used as a basis for textural analysis. Proportions of grains to matrix, carbonate to clays, and degree of lamination are included in the naming of the facies. The order of facies from base of Eagle Ford toward the upper section, indicates a succession from mudstones to laminated wackestone/packstone facies. Thus, the geologic facies are not independent of stratigraphy and depositional environment (Harbor, 2011; Fairbanks, 2012; and Workman, 2013). Furthermore, these authors describe facies in several wells located in different parts of the basin, showing a high degree of variation in the field. Present ash beds (usually less than 2 in (5 cm) thick) in the Eagle Ford are classified as massive bioturbated or bentonitic claystones with very high clay content. The packstone-

grainstone facies are limestone beds (up to 2 ft (2/3 m) thick), composed of over 75% calcite. Minerals found in the Eagle Ford formation mainly consist of calcite, dolomite, quartz, plagioclase, mixed layer clays, and pyrite (Jennings and Antia, 2013). Additionally, minor amounts of dolomite, plagioclase, feldspars and apatite are reported. The breakdown of clay minerals show high percentages of illite mixed layers, kaolinite and minor chlorite content. **Table 1** summarizes the lithofacies and mineralogy reported by the most recent Eagle Ford publications by Harbor (2011), Fairbanks (2012), and Workman (2013).

		Mineralogy (wt%)			
Facies	**Source**	**Calcite**	**Quartz**	**Clays**	**TOC (wt%)**
Massive Bentonitic Claystone	Fairbanks (2012)	< 5%	< 5%	90%	
Massive to Bioturbated Kaolinitic Claystone	Harbor (2011)	< 1 %	< 10 %	90%	
Massive to Bioturbated Claystone	Workman (2013)	30%	5%	45%	
Massive Argillaceous Mudrock	Harbor (2011)	25%	30%	45%	5%
Massive Argillaceous Mudrock	Fairbanks (2012)	35%	15%	55%	
Massive Argillaceous Foraminiferal Mudrock	Fairbanks (2012)	50%	15%	40%	
Laminated Argillaceous Mudstone	Workman (2013)	25%	20%	45%	3%
Laminated Argillaceous Foraminiferal Mudstone	Fairbanks (2012)	60%	10%	25%	
Weakly Laminated Calcareous Foraminiferal Mudstone	Workman (2013)	60%	15%	20%	3.5%
Laminated Wackestone	Harbor (2011)	65%	15%	20%	2%
Laminated Foraminiferal Wackestone	Fairbanks (2012)	75%	10%	10%	
Bioturbated Skeletal Lime Wackestone	Workman (2013)	85%	5%	5%	1%
Bioturbated Lime Wackestone	Harbor (2011)	90%	5%	5%	1%
Laminated Fossiliferous Wackestone/Packstone	Harbor (2011)	55%	15%	30%	7%
Disrupted Bedded Foraminiferal Packstone	Harbor (2011)	60%	10%	30%	8%
Massive Inoceramid Packstone	Harbor (2011)	70%	5%	25%	
Laminated Foraminiferal/Peloidal Packstone	Harbor (2011)	70%	10%	20%	4.5%
Skeletal Packstone/Grainstone	Workman (2013)	80%	5%	10%	1%
Foraminiferal Packstone/Grainstone	Workman (2013)	85%	10%	5%	0.5%
Nodular Foraminiferal Packstone/Grainstone	Fairbanks (2012)	85%	5%	10%	
Cross-laminated Foraminiferal Packstone/Grainstone	Fairbanks (2012)	90%	5%	5%	

Table 1. Eagle Ford geological facies description (Modified from Harbor, 2011; Fairbanks, 2012; Workman, 2013)

A previous study by Tian et al. (2013) showed that the production rates and fluid types of the Eagle Ford wells are correlated with formation depth and kerogen thermal maturity. The depth of the Eagle Ford formation increases from outcrops to the Edwards and Sligo shelf margins where it exceeds 15,000 ft. Structural dip is towards the southeast; Dip magnitude in the Maverick Basin on the south is less than dip at the San Marcos Arch. From northwest to southeast, as the maturity increases with depth, and hydrocarbon composition evolves from black oil to volatile oil, gas condensate, and finally dry gas. The most productive oil wells produced more than 16,000 bbl/month in Karnes and Gonzales counties. The average gas-oil-ratio (GOR) of black oil wells was reported approximately 1,000 SCF/bbl (Tian et al., 2013). By integration of limited PVT data and formation vertical depth, Tian et al. (2014) created a regional map that illustrates northeastward increase in reservoir pressure gradient from 0.68 psi/ft in the Maverick Basin to 0.85 psi/ft in Karnes County.

Wells 1 and 2 in this study **(Figure 1)** are located in the oil window of Eagle Ford formation, just north of Edwards Reef Margin. Based on previously published literature, and interpretation of well-logs, the upper Eagle Ford (UEF) section appears to be less than 40 ft in this area, as it is truncated beneath the unconformity at the base of Austin Chalk (Donovan and Staerker, 2010; Workman, 2013; Hentz and Ruppel, 2010). The total thickness of the lower Eagle ford interval is approximately 145 feet in Well 1 and 125 feet in Well 2; it consists of laminated organic-rich marlstone-limestone laminae. Available rock data for these wells cover the lower Eagle Ford, which is organic-rich and known to be the most productive interval in the formation. Triple-

combo, spectral gamma ray, and ECS logs in addition to core measurements such as XRD and Rock-Eval Pyrolysis, thin-section images, and depth-by-depth XRF measurements were acquired for this study.

Rock-Eval pyrolysis measurements show a vertical variation in organic properties such as TOC, hydrogen index (HI), and thermal maturity. Type II oil-prone kerogen is present in Well 1, with Tmax values in the range of 430-450 °C. Calcite, quartz, illite mixed layers, and kaolinite are dominant minerals in the depth intervals of interest. Furthermore, XRD measurements show pyrite weight concentrations as great as 5%. The breakdown of clay minerals indicates presence of illite-smectite and illite-mica layers at the upper portion of LEF, whereas the base of LEF contain a mixture of illite and kaolinite.

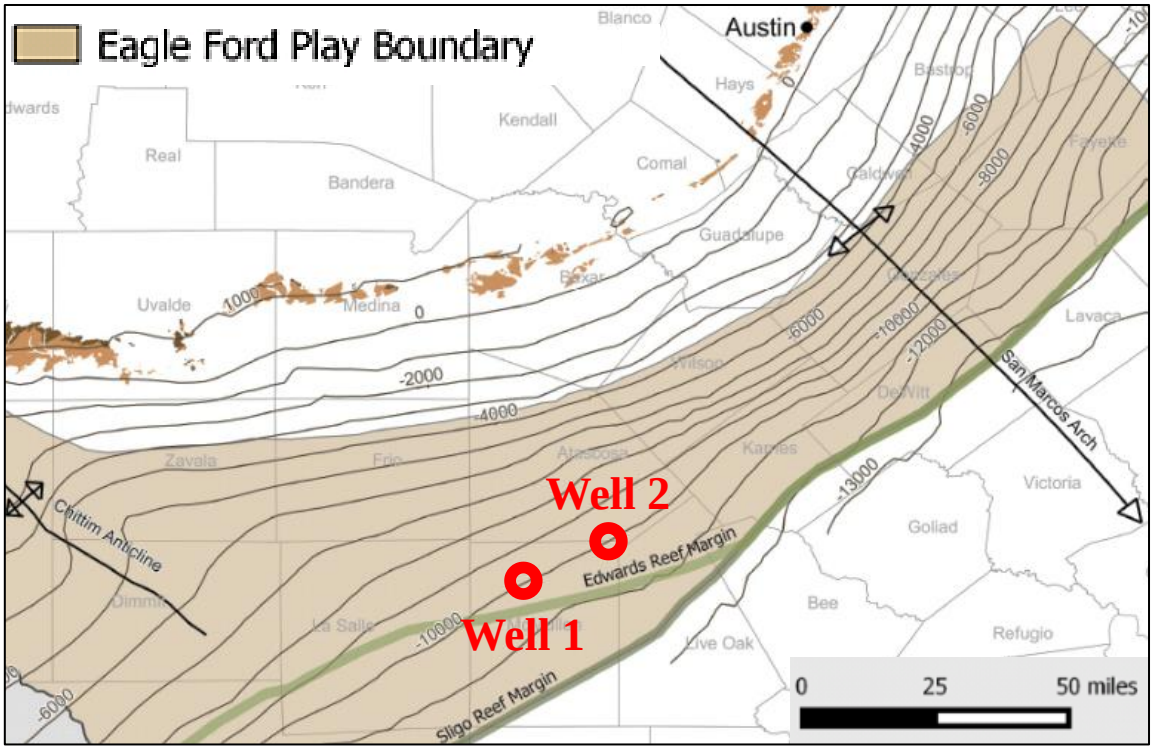

Figure 1. Location of Wells 1 and 2, just north of the Edwards Shelf Margin (Modified from EIA, 2014).

3.2 Petrophysical Evaluation

I first estimated petrophysical and compositional properties in the LEF section of Wells 1 and 2. I used triple-combo and ECS logs as inputs to calculate depth-by-depth volumetric concentration of minerals and petrophysical properties such as porosity and fluid saturations. I determined output minerals based on 10 uniformly distributed X-ray diffraction samples (average 15 feet per sample) in the lower Eagle Ford interval. To reduce inversion errors, I utilized element-to-mineral correlations that was obtained through laboratory measurements of XRF and XRD on the same sample. I incorporated

two element-mineral relationships with correlation coefficient of greater than 0.95 as constraints in the inversion process:

1) Calcium (wt%) vs. Calcite (v/v): the correlation is expected since dolomite is present in very minor amounts in this well.
2) Potassium (wt%) vs. Illite Mixed Layers (v/v): Illite is the only mineral that is composed of approximately 6 weight percent of potassium

Figure 2 shows the comparison of the mineral concentrations against the core XRD measurements. Furthermore, Tracks 2-8 of **Figure 3** and **Figure 4** show the well-logs and well-log based estimates of petrophysical and compositional properties in Wells 1 and 2, respectively.

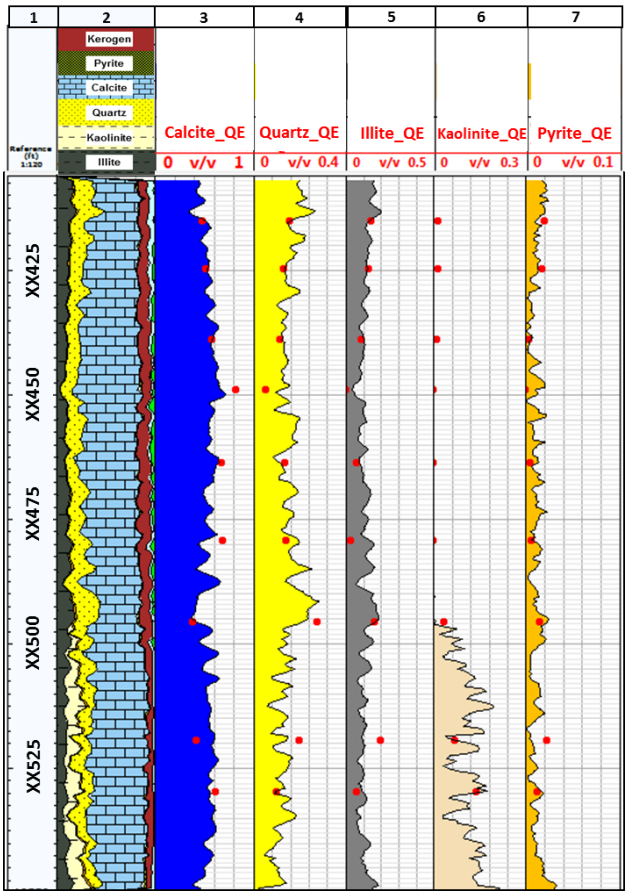

Figure 2. Validation of mineral volumetric concentrations against core XRD measurements in the LEF interval of Well 1. Tracks from left to right include, Track 1: depth (ft); Track 2: cumulative volumetric concentrations of minerals and fluids; Track 3-7: volumetric concentrations

Then, I applied the SCA technique to estimate depth-by-depth elastic moduli such as bulk and shear modulus, taking into account the mineral volumetric concentrations and their associated grain shape factors (α). I determined the possible ranges for individual elastic moduli of the constituents from published literature (Mavko et al., 2009; Prasad et al., 2002; Sone et al., 2013; Vanorio et al., 2003), while the mineral shape factors were obtained using X-ray elemental maps.

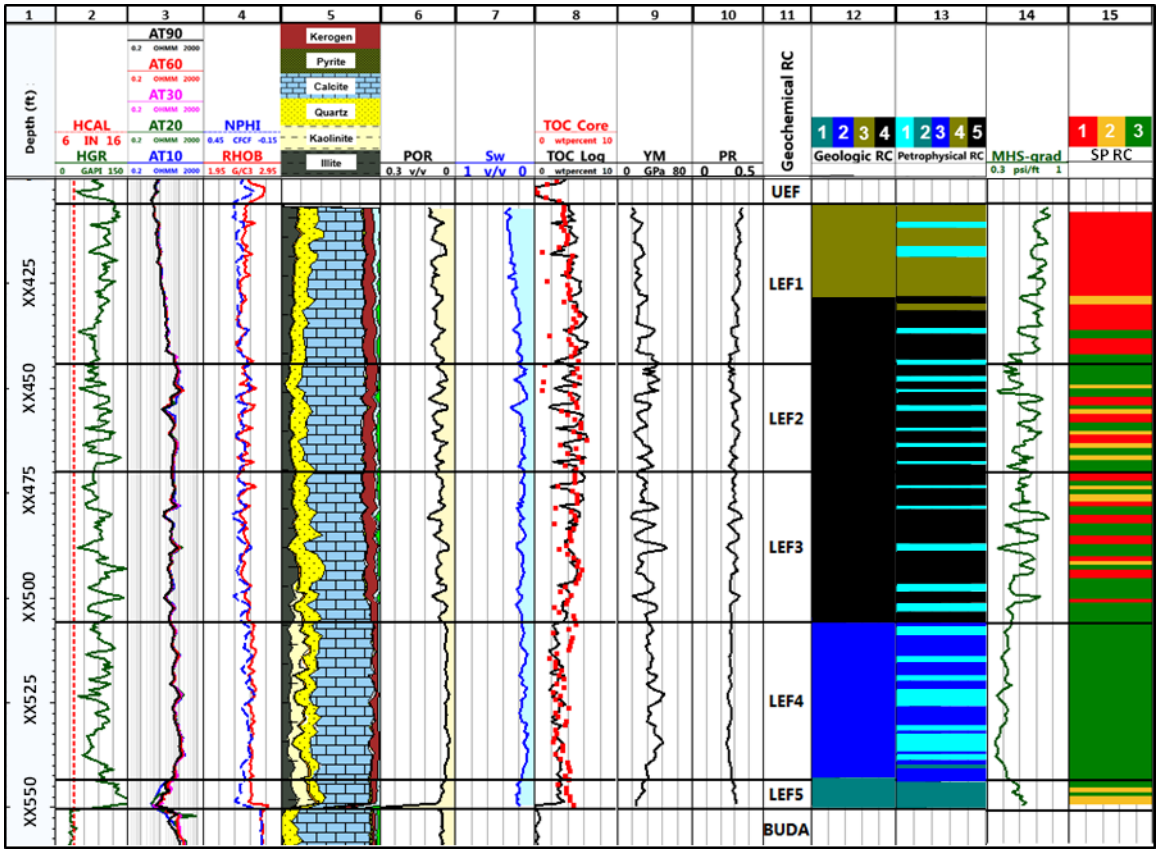

Figure 3. Well 1, Lower Eagle Ford example. Conventional well-logs, estimates of petrophysical, compositional and elastic properties, and the results of geochemical, geological, petrophysical, and geomechanical classifications. Tracks from left to right include, Track 1: depth; Track 2: high resolution GR (HGR), caliper (HCAL); Track 3: array induction resistivity logs (AT10-AT90); Track 4: neutron porosity (in water-filled limestone units, NPHI) and bulk density (RHOB); Track 5: estimates of volumetric concentrations of minerals; Track 6: estimates of total porosity (POR); Track 7: estimates of water saturation (Sw); Track 8: well-log-based estimates of TOC (derived from bulk density log) compared to core measurements; Track 9: estimates of Young's modulus (YM); Track 10: estimates of Poisson's ratio (PR); Track 11: outcome the of geochemical rock classification; Track 12: outcome of the geological rock classification; Track 13: outcome of the well-log based petrophysical rock classification (PRC); Track 14: estimates of minimum horizontal stress gradient (MHS); Track 15: outcome of the rock classification based on stress-profiles (SPRC).

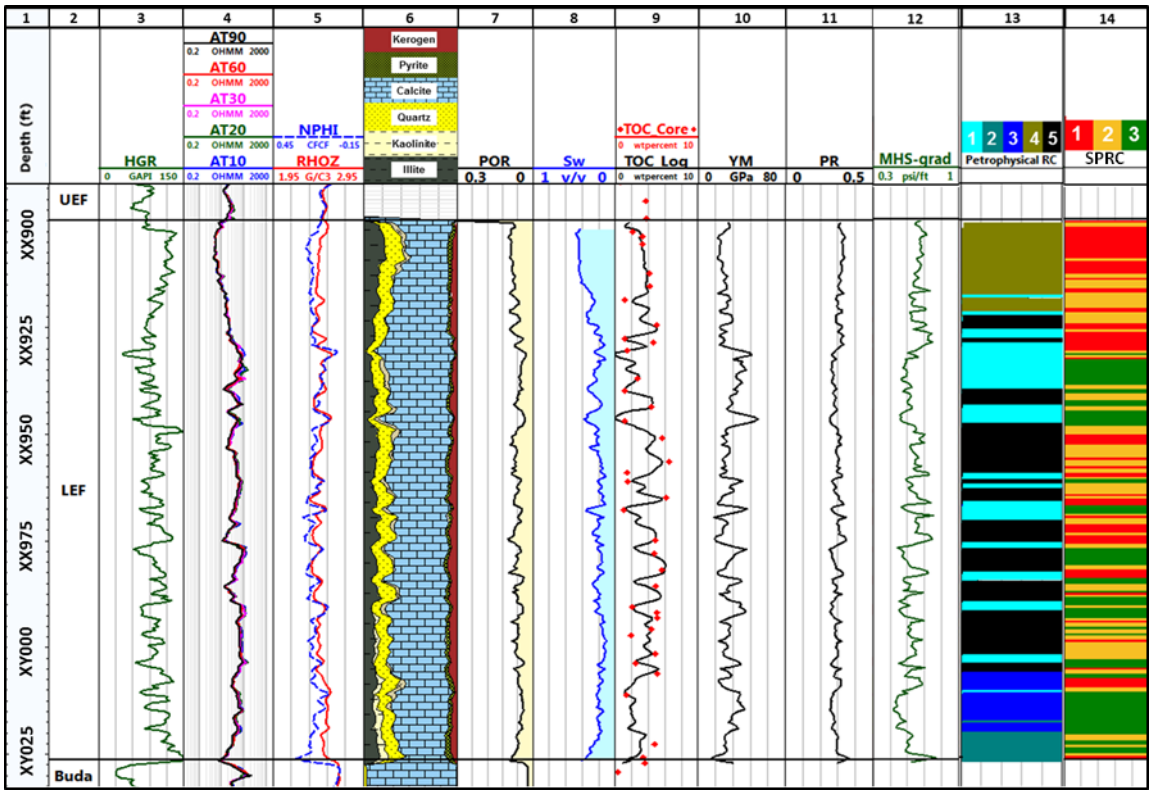

Figure 4. Well 2, Lower Eagle Ford example. Conventional well-logs, estimates of petrophysical, compositional and elastic properties, and the results of the petrophysical and geomechanical classifications. Tracks from left to right include, Track 1: depth; Track 2: high resolution GR (HGR); Track 3: array induction resistivity logs (AT10-AT90); Track 4: neutron porosity (in water-filled limestone units, NPHI) and bulk density (RHOZ); Track 5: estimates of volumetric concentrations of minerals; Track 6: estimates of total porosity (POR); Track 7: well-log-based estimates of water saturation compared to core measurements (S_w); Track 8: well-log-based estimates of TOC (derived from bulk density log) compared to core measurements; Track 9: estimates of Young's modulus (YM); Track 10: estimates of Poisson's ratio (PR); Track 11: outcome of the well-log based petrophysical rock classification (PRC) based on estimates of total porosity, water saturation, total organic carbon, total clay volume, Young's modulus, and Poisson's ratio; Track 12: estimates of minimum horizontal stress gradient (MHS); Track 13: outcome of the well-log based petrophysical rock classification (PRC) based on estimates of total porosity, water saturation, total organic carbon, total clay volume, Young's modulus, and Poisson's ratio; Track 14: outcome of the rock classification based on stress-profiles (SPRC).

Figure 5 shows examples of core X-ray elemental distribution images from the LEF. Quartz and pyrite appeared to be more spherical shaped. Aspect ratio (α) of 1 is assigned to these minerals. On the other hand, for clay minerals where the structure consists of nanometer scale layers, I assigned an aspect ratio of 0.01. Calcite grains appear to be elliptical and to be compacted and interbedded with clays at some zones, but in other zones are more spherical. Therefore, I assigned two different shape factors for calcite constituent (i.e., 0.1 for elliptical and 1 for spherical grains).

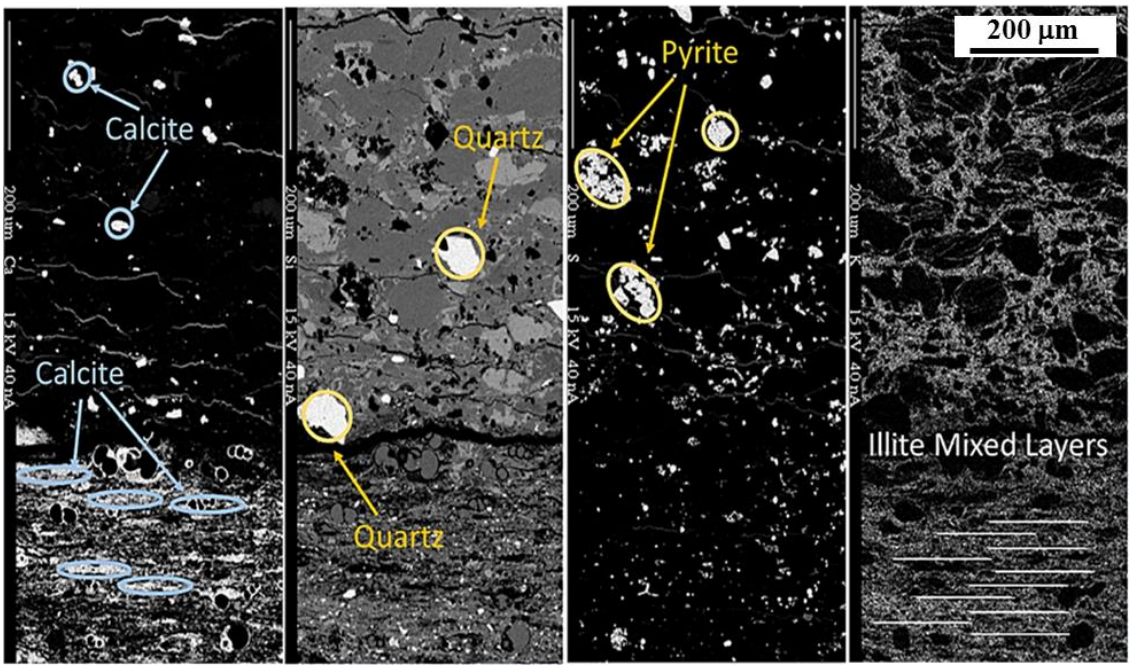

Figure 5. Mineral grains identified using 2D X-ray elemental distribution maps from the lower Eagle Ford core samples.

Table 2 shows the input constants that minimized the difference between estimated acoustic-wave slowness and those from acoustic well logs in the wells where

acoustic measurements are available (e.g., Well 2). The same input parameters are used in the wells where acoustic measurements are not recorded to estimate elastic properties.

SCA Parameters	Calcite (spherical)	Calcite (elliptical)	Quartz	Pyrite	Illite	Kaolinite	Kerogen
K (GPa)	75	75	38	147	8	6	5
μ (GPa)	40	40	44	132	6	2	3
α	1	0.1	1	1	0.01	0.01	0.1

Table 2. Input parameters to the SCA model, lower Eagle Ford

Figure 6 shows the estimates of petrophysical and compositional properties, as well as comparison between the well-log measurements of compressional-wave slowness (DTCO), and shear-wave slowness (DTSH), with the estimated compressional- and shear-wave slowness from SCA method in Well 2. The SCA results provide a higher resolution assessment of acoustic compressional- and shear-slowness. Although, higher errors in estimates of shear-wave slowness was observed, the approximation remained reliable for majority of the depth intervals. Due to limited number of X-ray images, I used a single model for the LEF interval. However, availability of large number of high resolution core images can potentially enable the assignment of zonal shape factors based on rock facies classification, resulting in a more robust and reliable model. After application of the calibrated SCA model to Well 1 and Well 2, I estimated depth-by-

depth values of YM and PR. Tracks 9-10 of Figure 3 and Figure 4 show the final estimates of YM and PR in Well 1 and Well 2, respectively.

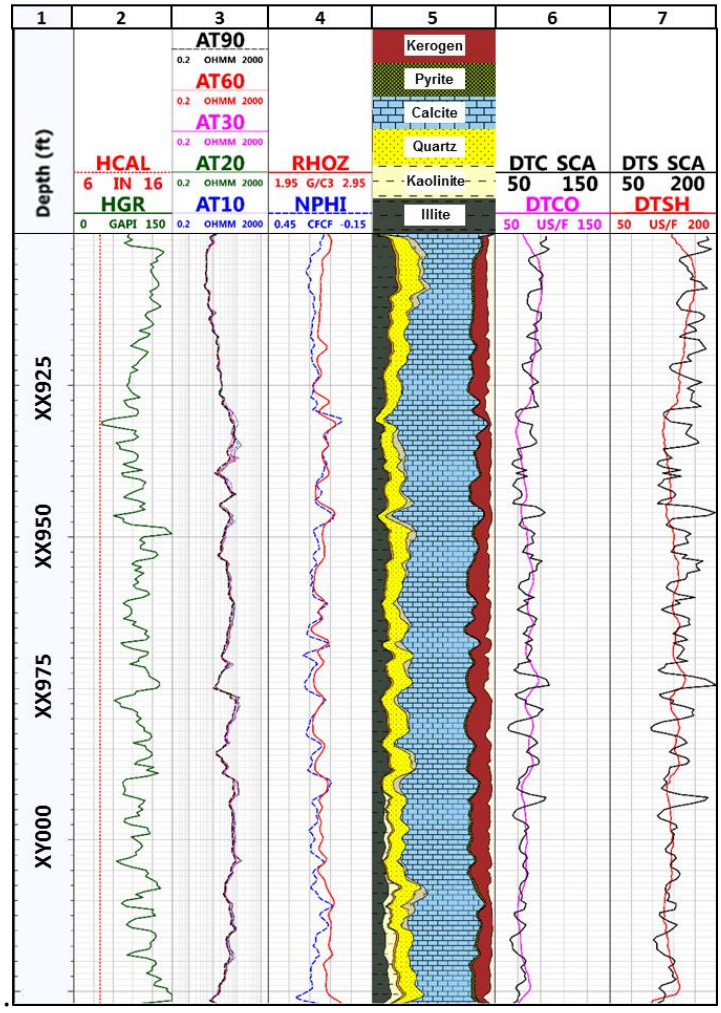

Figure 6. Well 2, Lower Eagle Ford Field example: conventional well-logs, estimates of volumetric concentration of minerals, and acoustic well-logs. Tracks from left to right include, Track 1: depth; Track 2: high resolution GR, caliper; Track 3: array induction resistivity logs; Track 4: neutron porosity (in water-filled limestone units), bulk density; Track 5: estimates of volumetric concentrations of minerals; Track 6: SCA-based estimates of compressional-wave slowness compared to the acoustic well-log measurement (DTCO); Track 7: SCA-based estimates of shear-wave slowness compared to the acoustic well-log measurement (DTSH).

3.3 Chemostratigraphy of Lower Eagle Ford

We divided the lower interval of Eagle Ford formation into five geochemical classes (LEF1 to LEF5 in descending order; **Figure 7**), based on significant stratigraphic variations in major elements (Ca, Si, Al, K, Fe, S), trace elements (U, V, Ni, Mo), and total organic carbon concentrations. Figure 7 shows depth-by-depth core XRF measurements obtained in the lower Eagle Ford in Well 1, as well as the geochemical rock classification results. Through analysis of the results, we highlight distinguishing geochemical characteristics among the classes. The lowest unit, LEF5, immediately above the Buda Limestone, is chemostratigraphically distinct. Uranium content is greatest in this interval, and the Si/Al ratio is very low (~1.5-3.0). In terms of organic geochemistry, TOC is moderate to high (4-5 wt%). LEF4 is distinguished by its low TOC content (2-4 wt%). LEF3 is similar to LEF4, except it contains higher TOC (> 4 wt%), and lower calcium (Ca) content. LEF2, has significantly higher concentrations of trace elements vanadium (V), nickel (Ni), molybdenum (Mo), and uranium (U), than are in the underlying units. LEF1 has a linearly decreasing Ca content, and likewise, increasing Al and Si content. Vanadium concentration is similar to LEF2, and a significant decrease in nickel concentration is present. **Table 3** lists class-by-class distribution of the elemental concentrations (i.e., S, U, V, Ni), and total organic content (TOC), that were used as the basis of discrimination between the geochemical classes. Track 11 of Figure 3 shows the identified chemostratigraphic units in Well 1.

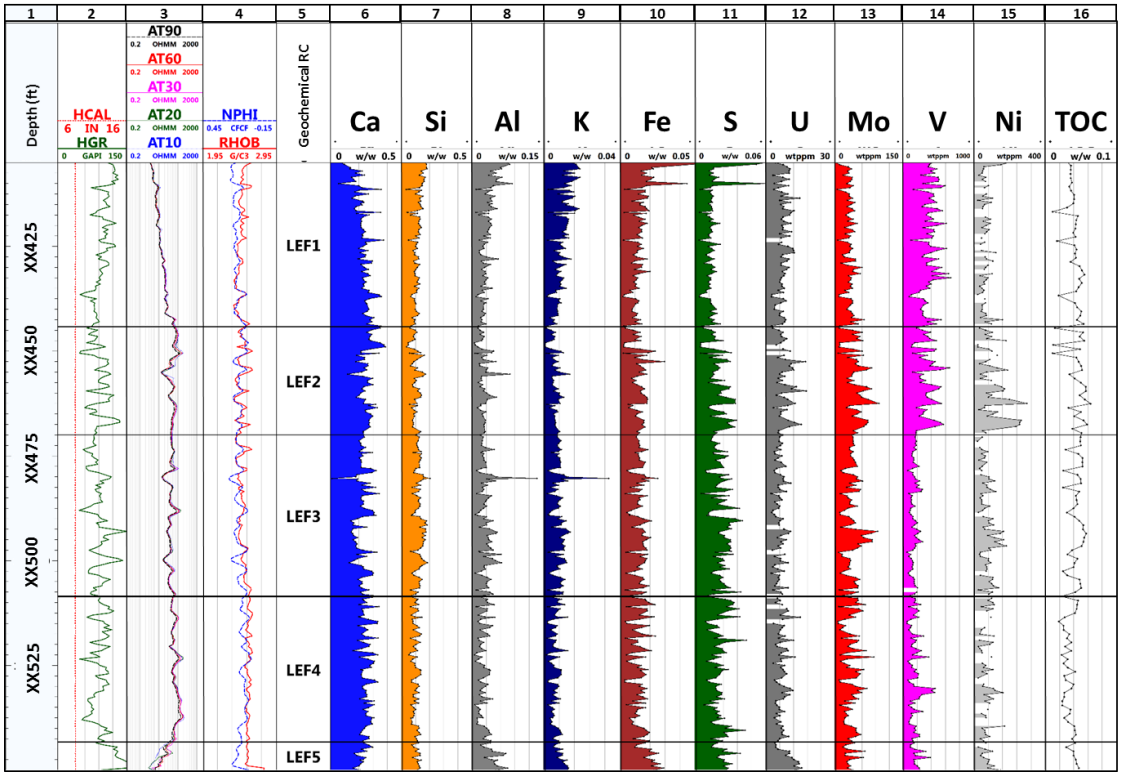

Figure 7. Well 1, Lower Eagle Ford Field example. Conventional well-logs, and vertical distribution of concentrations of major and trace elements in the lower Eagle Ford used to divide the section into five chemostratigraphic units. Tracks from left to right include, Track 1: depth; Track 2: Chemostratigraphy of lower Eagle Ford; Track 3: high resolution GR; Track 4: array induction resistivity logs; Track 5: neutron porosity (in water-filled limestone units), bulk density; Tracks 6-15: calcium (Ca), silicon (Si), aluminum (Al), potassium (K), iron (Fe), sulfur (S), uranium (U), molybdenum (Mo), vanadium (V), and nickel (Ni) weight concentrations obtained from core XRF measurements; Track 16: total organic carbon weight concentration (LECO™ TOC measurements).

The key petrophysically relevant observations from the chemostratigraphic analysis are summarized as follows.

While the dominant clay type is illite mixed layers for most of the LEF, the significant exception is the lowermost units (LEF5 and to a lesser extent, LEF4). Kaolinite is significant in the LEF5, as presented by the very low Si/Al ratio (<2), and low potassium (0.2- 0.3 wt%). These characteristics indicate that illite is diluted by the presence of a clay that is not potassic, with a lower silicon content.

Geochemical RC	S (wt%)	U (ppm)	V (ppm)	Ni (ppm)	TOC (wt%)
LEF1	1.4 ± 0.2	7.0 ± 1.3	404 ± 102	64 ± 24	4.3 ± 0.6
LEF2	2.3 ± 0.6	7.5 ± 1.3	391 ± 112	126 ± 65	5.0 ± 0.8
LEF3	2.5 ± 0.7	6.2 ± 1.7	176 ± 61	81 ± 37	4.4 ± 0.9
LEF4	2.2 ± 0.5	6.9 ± 1.5	207 ± 97	70 ± 33	3.0 ± 0.5
LEF5	2.6 ± 0.6	12 ± 2.0	192 ± 62	75 ± 34	4.1 ± 0.4

Table 3. Distribution of core XRF measurements of elemental weight concentrations separated by geochemical rock class in Well 1.

LEF1 and LEF2 appear to be associated with intervals of extreme enrichment of specific trace metals including V and Ni. These two elements, along with U and Mo, are considered to be useful indicators for productivity and preservation of organic matter, as well as for different types of anoxia (Tribovillard et al., 2006; Wilde et al., 2004). According to Lewan (1984), when anoxia is strong enough to cause episodic or persistent sulfur-reduction (in sediments or within the water column), the chemical reduction of trace elements (i.e. Mo, U, and V) is enhanced, and they can be

incorporated into the sediments in the presence of sufficient organic matter. One implication is that V and Ni concentrations, and their relative proportions can convey information about kerogen type and presence of trapped hydrocarbons. **Figure 8** through **Figure 10** show a class-by-class distribution of the Rock-Eval parameters including *S1*, *HI*, and T_{max}. The *S1* and *S2* values from Rock-Eval measurements confirm that hydrocarbon content is high when V and Ni are high. The concentrations of trace elements appeared to correspond more closely with hydrocarbon content, compared to TOC.

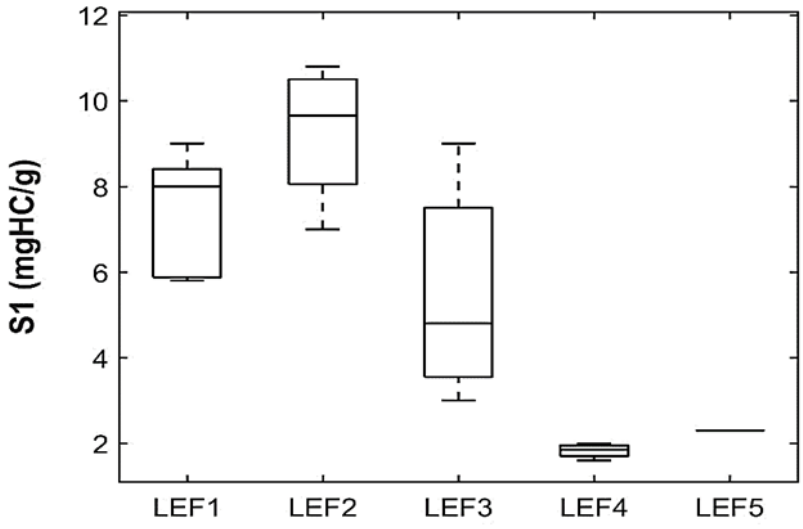

Figure 8. Distribution of *S1* (free hydrocarbon content) from Rock-Eval pyrolysis, separated by geochemical class.

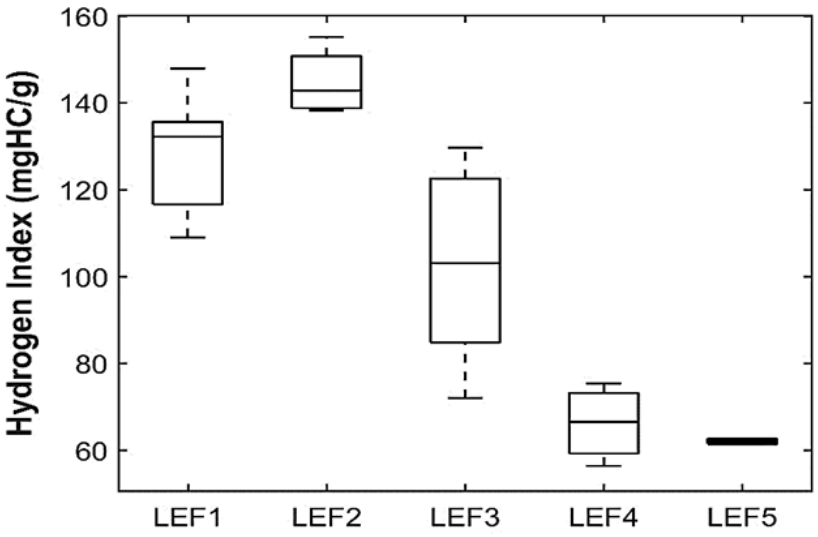

Figure 9. Distribution of *HI* (hydrogen index) from Rock-Eval pyrolysis test, separated by geochemical class.

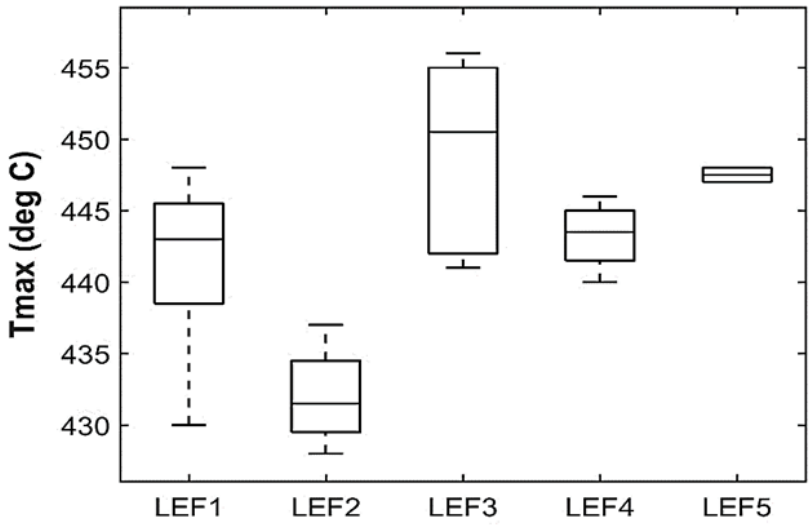

Figure 10. Distribution of T_{max} from Rock-Eval pyrolysis test, separated by geochemical class.

3.4 Lithofacies Classification

Through the analysis of thin-sections and core images obtained from 145 feet of conventional, we identified four lithofacies in the lower Eagle Ford interval. This classification takes into account the mineralogy, texture, grain-to-matrix ratio, fossil types, and sedimentary structures observed in the core. Track 12 of Figure 3 show the lithofacies classification from Well 1. From the base of the Eagle Ford, an upward LEF strata evolve from a massive or weakly laminated texture, to repetitive, alternating pair of lithofacies that dominates the majority of the Lower Eagle Ford section. The pair consists of two main sub-facies: foraminiferal mudstone and packstones. These facies alternate at different thickness scales from sub-millimeter up to decimeter. Furthermore, mixtures of these facies are common depending on the scale of observation. Typically, this pair of facies has minimal or no bioturbation and boundaries between facies are sharp. The foraminiferal mudstones consists of bioclastic grains (10-100 microns), carbonate mudstone and clays. The bioclastic grains are mostly foraminiferal tests but may include skeletal remains of ostracodes, diatoms, and bivalves. Perhaps with the exception of bivalves, the bioclastic grains in the Lower Eagle Ford are planktonic with no benthic tests reported to date (Lowery et al., 2014).

The packstone-grainstones are essentially composed of planktonic foraminifera but without significant clays or other siliciclastics. They tend to be in light grey color. Diagenetic packstone-grainstones look much like the regular packstone-grainstones but record many diagenetic events and features including recrystallization, calcite cement,

concretions, and dolomitization. **Figure 11** shows core photographs of representative lithofacies.

The four identified lithofacies in the Lower Eagle Ford include massive argillaceous mudstone, laminated argillaceous foraminiferal mudstone, bedded foraminiferal mudstone/nodular limestone, bedded foraminiferal wackestone/limestone, which are described as follows.

Lithofacies 1. Massive argillaceous mudstone. These mudstone facies with little or no discernable bedding structures are present at the base of Eagle Ford. Few foraminifera are identified in these mudstones, and clay content consisting of illite mixed layers and kaolinite is high compared to other lithofacies.

Lithofacies 2. Laminated argillaceous foraminiferal mudstone. These facies have a medium grey color due to the millimeter-scale interlamination of mudstone with foraminiferal limestone laminae. Commonly, the proportions of mudstone to foraminifera-rich limestone change in these facies. Mineralogy from XRD measurements indicate carbonate content as low as 45%, and total clay (illite and kaolinite) content as much as 30% in volume.

Lithofacies 3. Bedded foraminiferal mudstone/nodular limestone. Dark-gray to black illite-rich mudstones with faint laminations, where the limestone beds are nodular (carbonates nodules described by Dawson, 2000). Commonly, internal structures of the nodular limestones are obliterated by pore-filling cementation and recystrallization. Transitions between mudstones and limestones are sharp. Moreover, since the bounding

surfaces of the nodular laminations are often curved, it is possible in that in some cases, the nodular limestones are laterally discontinuous.

Lithofacies 4. Bedded foraminiferal wackestone/limestone. The wackestone is dark grey to black due to high (4-6 wt%) organic content. Wackestones contain thin foraminiferal lags and isolated bivalves. Limestone beds with thickness of few inches to a foot, are foraminiferal packstone and grainstones transitioning at sharp boundaries with the wackestones. The abundance of bioclastic grains in this lithotype is higher relative to the deeper mudstone facies (Lithofacies 1 and 2).

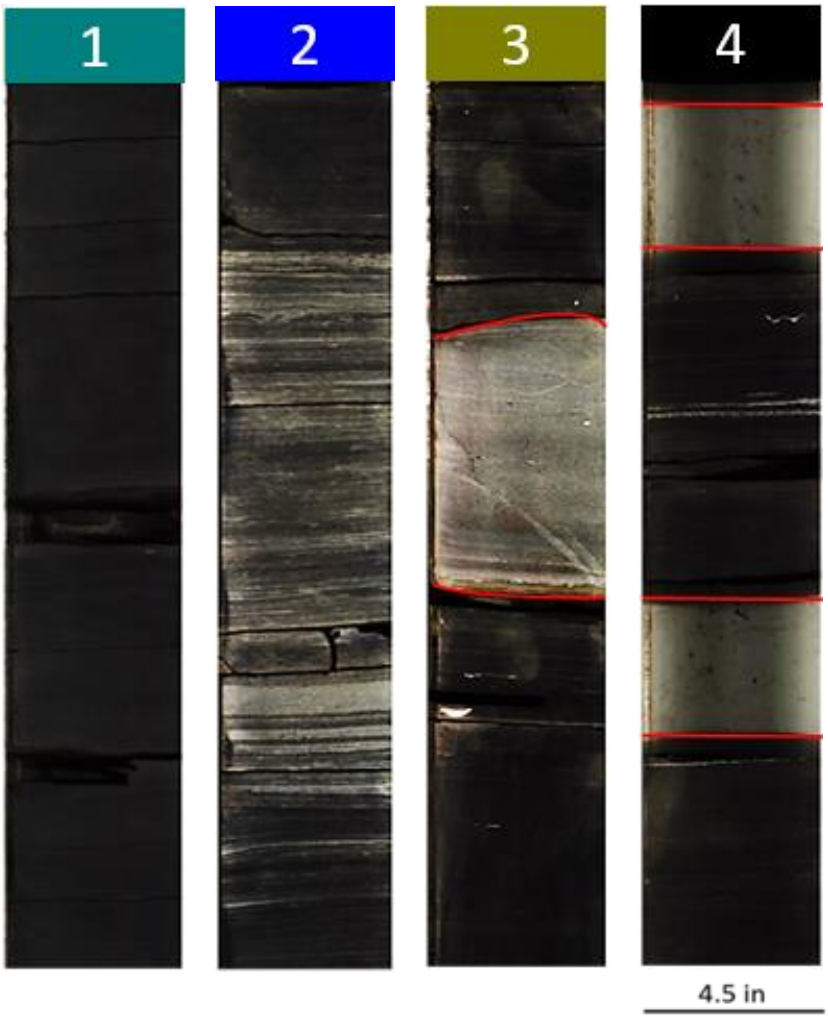

Figure 11. Examples of core images associated with lithofacies 1-4 in the lower Eagle Ford, from Well 1.

Figures 12 through **16** show different examples of the thin-section images of foraminiferal packstone/grainstone, wackestone and mudstone facies. These images show a variations in the proportions of bioclastic grains to mud. Foraminifers are the most abundant fossils in the lower Eagle Ford formation, and are composed of calcite. In

some cases, they are affected by dissolution. Due to the organic-richness of the rocks, the color of the matrix mud is dark grey to black. Based on Dunham's carbonate classification, the grain-to-matrix ratio is over 90 % for packstones and grainstones. This ratio in wackestones is between 10-90 %, and less than 10 % for mudstones (Dunham, 1962).

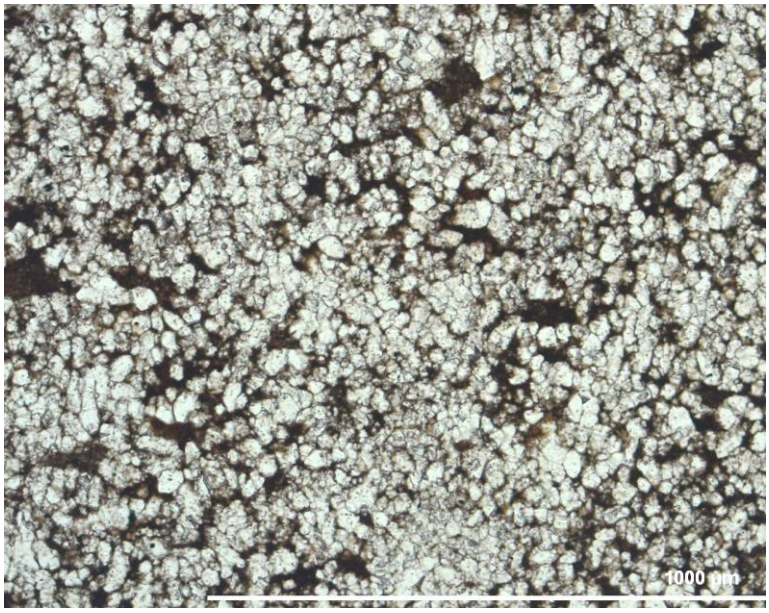

Figure 12. Thin-section example of foraminiferal packstone/grainstone facies, associated with a limestone nodule at the top of LEF.

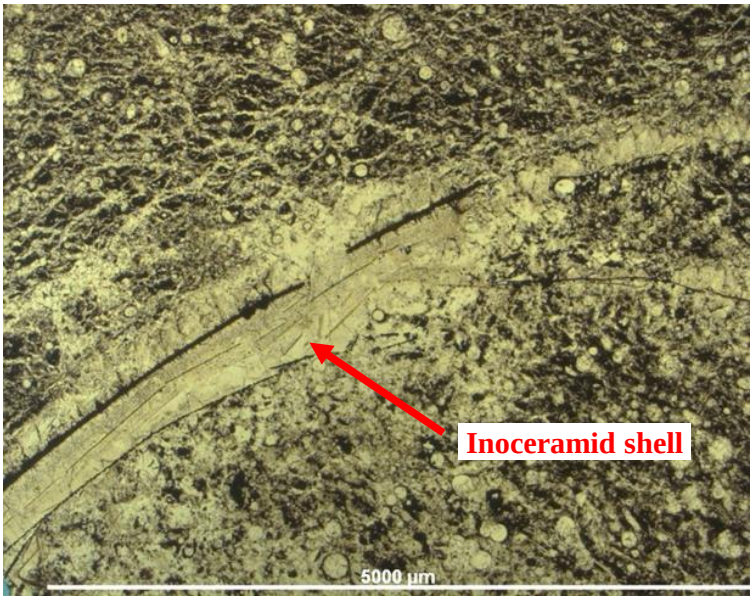

Figure 13. Thin section example of skeletal packstone facies observed from the LEF; an inoceramid shell is present.

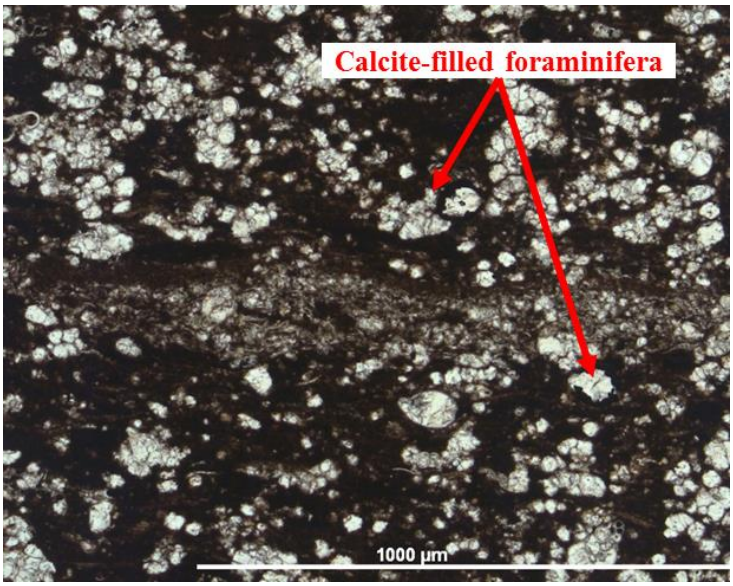

Figure 14. Thin-section example of foraminiferal wackestone facies in LEF; calcite-filled forams are abundant.

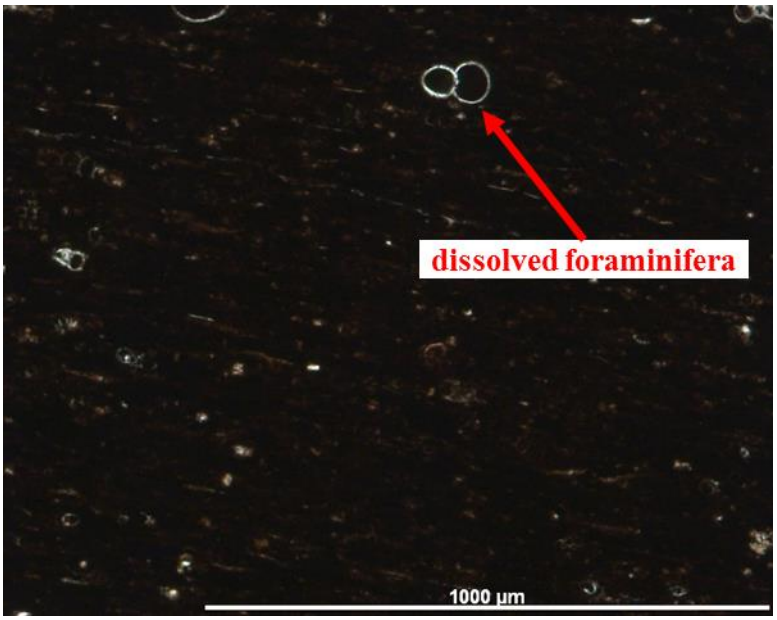

Figure 15. Thin-section example of foraminiferal mudstone facies in the lower Eagle Ford. Dissolved forams are present.

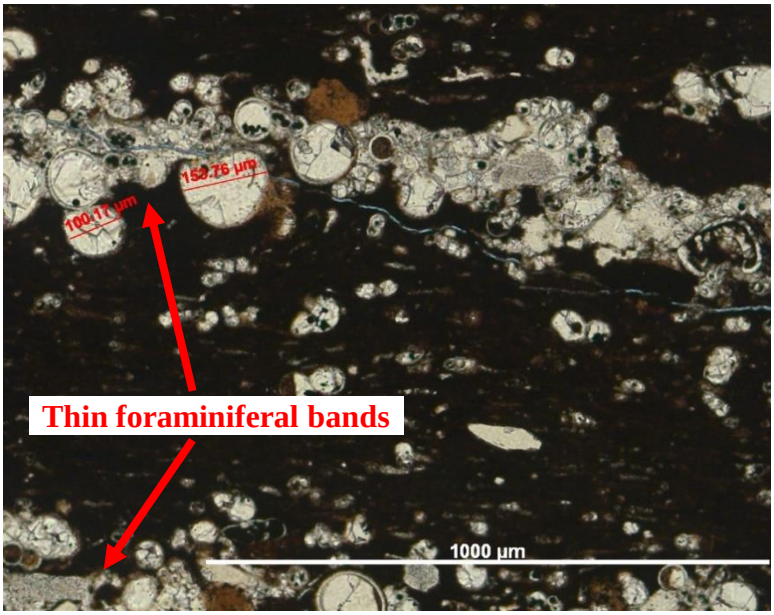

Figure 16. Thin-section example of laminated foraminiferal mudstone facies. Sub-millimeter foraminiferal bands are evident.

3.5 Petrophysical Rock Classification (PRC)

Inputs to this well-log-based classification include porosity, water saturation, TOC, total clay volume, Young's modulus, and Poisson's ratio. Track 13 of Figure 3, and track 11 of Figure 4, show the petrophysical classification results from analysis of Wells 1 and 2, respectively. Furthermore, **Figures 17** through **19** are cross-plots of the estimates of petrophysical and compositional properties for both wells. **Tables 4** and **5** include class-by-class statistics of the well-log-based classification results from Wells 1 and 2, respectively.

I ranked the petrophysical classes using an integrated rock characterization approach. To fully characterize the petrophysical classes, I integrated the results of the previously described geological and geochemical classifications with the results of petrophysical classification, presented in this section. The characteristics of petrophysical rock classes are described as follows.

PRC1 occurs interbedded throughout the rock classes, with exception of the massive argillaceous mudstones. Geologically, this class is a carbonate with low porosity and occurs interbedded with other PRCs.

PRC2 corresponds to the massive argillaceous mudstones. This class is notable for kaolinite content up to 14% (vol%). TOC can be as great as 4.0 wt% but the rock contains small volumes of free hydrocarbon (maximum S1 peak from core was 2.6 mgHC/g in Well 1).

PRC3 is associated with the laminated argillaceous foraminiferal mudstones. It appears to be a mudstone with low porosity and low TOC (i.e., less than 3 wt%).

PRC4 is interbedded with PRC1 in the bedded foraminiferal mudstone/nodular limestone. It is a porous (approximately 8.5% porosity) mudstone with moderate to high TOC content (3-5 wt%), and the lowest estimated Young's modulus among the other rock classes. The water saturation is the higher in this rock class with maximum value of 48% in Well 2.

PRC5 represents organic-rich foraminiferal wackestone facies. Petrophysically, it is similar to PRC4, contains the most hydrocarbon content (S1 between 7-11 mgHC/g) and lower water saturation estimates (maximum of 30%) relative to PRC4.

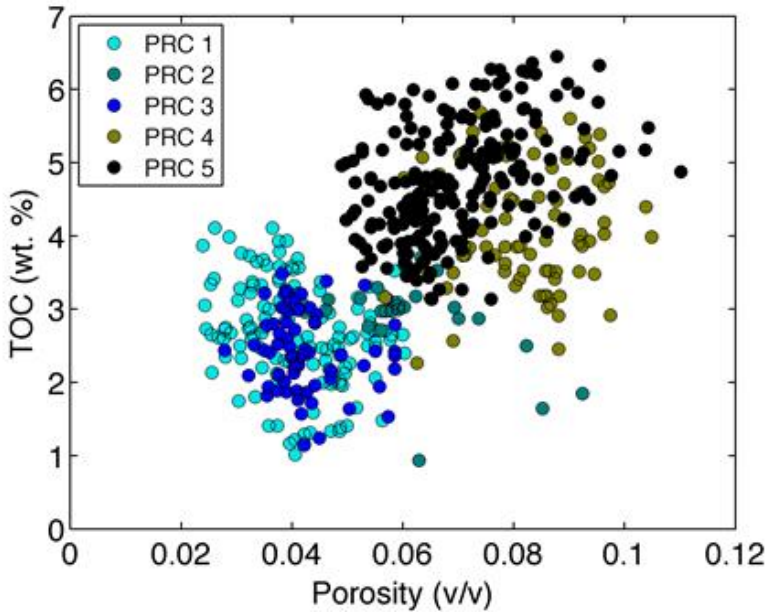

Figure 17. Well-log based estimates of TOC vs. porosity in Wells 1 and 2. Colors represent different petrophysical rock class.

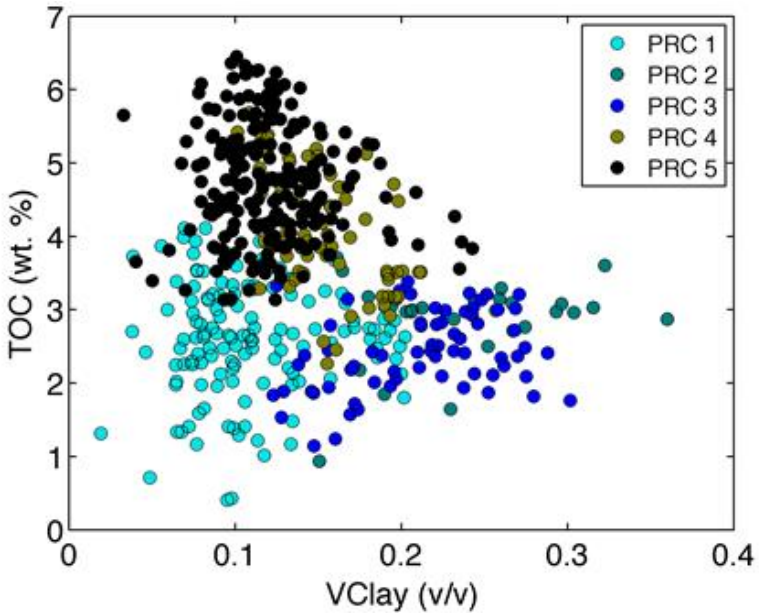

Figure 18. Well-log based estimates of TOC vs. volumetric concentration of clays in Wells 1 and 2. Colors represent different petrophysical rock class.

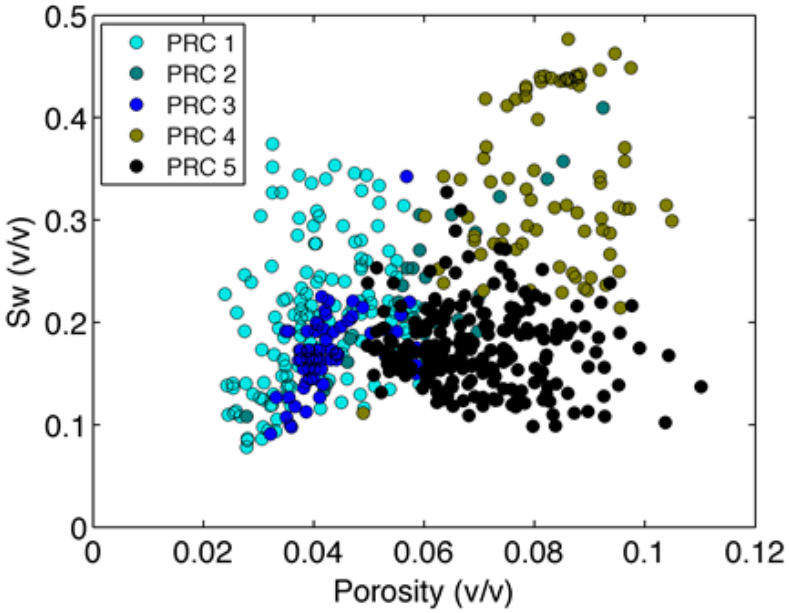

Figure 19. Well-log based estimates of water saturation vs. porosity in Wells 1 and 2. Colors represent different petrophysical rock class.

Petrophysical Rock Class	Porosity (%)	TOC (wt%)	Total Clay Volume (%)	Water Saturation (%)	Young's Modulus (GPa)	Poisson's Ratio
PRC1	3.5 ± 0.6	3.8 ± 0.8	12 ± 4	17 ± 7	39 ± 6	0.27 ± 0.01
PRC2	5.5 ± 0.8	2.8 ± 1.1	29 ± 4	20 ± 3	26 ± 4	0.29 ± 0.01
PRC3	3.9 ± 0.3	2.7 ± 0.5	24 ± 4	16 ± 3	34 ± 2	0.27 ± 0.01
PRC4	8.5 ± 1.1	4.8 ± 0.5	14 ± 2	28 ± 4	22 ± 2	0.33 ± 0.01
PRC5	7.0 ± 1.3	5.0 ± 0.7	12 ± 4	16 ± 3	28 ± 3	0.30 ± 0.01

Table 4. Well 1: class-by-class statistics of the well-log-based rock classification results from the LEF

Petrophysical Rock Class	Porosity (%)	TOC (wt%)	Total Clay Volume (%)	Water Saturation (%)	Young's Modulus (GPa)	Poisson's Ratio
PRC1	4.6 ± 0.8	2.1 ± 0.8	9 ± 3	28 ± 7	36 ± 6	0.28 ± 0.01
PRC2	6.6 ± 1.1	2.7 ± 0.7	20 ± 3	28 ± 6	26 ± 4	0.30 ± 0.01
PRC3	4.8 ± 0.7	2.4 ± 0.6	17 ± 2	30 ± 3	28 ± 5	0.30 ± 0.01
PRC4	8.1 ± 0.9	3.5 ± 0.4	20 ± 3	39 ± 6	23 ± 3	0.32 ± 0.01
PRC5	7.0 ± 1.0	4.5 ± 0.7	17 ± 3	18 ± 4	25 ± 3	0.30 ± 0.01

Table 5. Well 2: class-by-class statistics of the well-log-based rock classification results from the LEF

In determination of reservoir quality rock classes, I accounted for factors such as storage capacity, organic-richness, thermal maturity of kerogen, and free hydrocarbon content in the rocks. **Figure 20** shows Rock-Eval measurements of *S1* versus TOC in the LEF, separated by petrophysical class. It is evident from the data that high TOC by itself is not necessarily an indicator of a reservoir quality rock. For instance, at TOC concentrations of over 4 wt%, PRC5 and PRC4 generated significantly higher free hydrocarbons, comparing to PRC3 and PRC2.

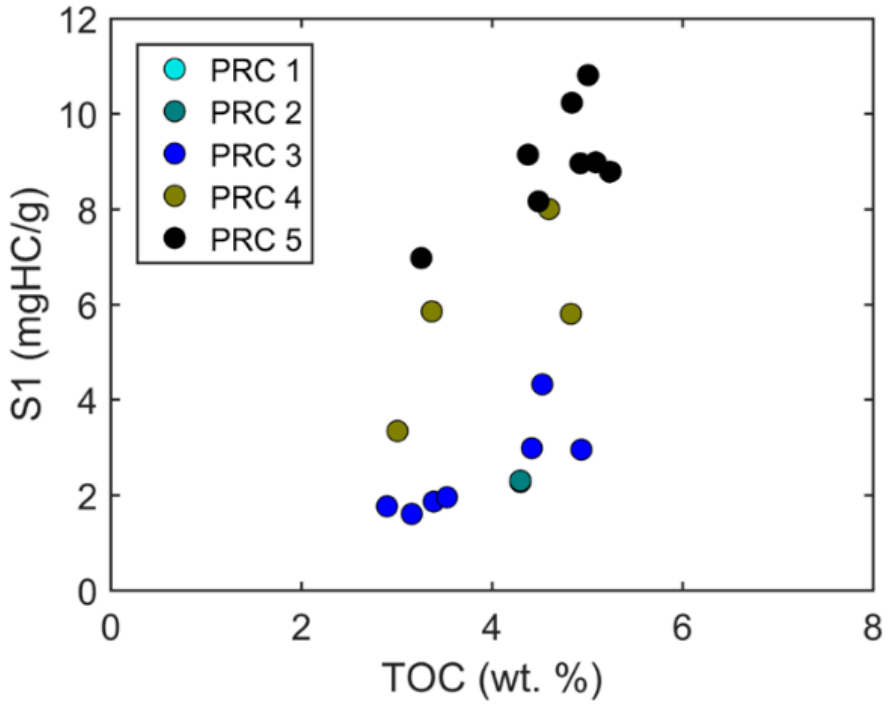

Figure 20. Well 1: Rock-Eval pyrolysis measurements of S1 versus TOC in the LEF. Different colors represent different petrophysical rock classes

3.6 Geomechanical Rock Classification Based on Stress-Profiles (SPRC)

After identifying the best reservoir quality rock classes in the formation, it is essential to conduct a geomechanical evaluation to ensure the ability to create effective fracture networks as pathways for hydrocarbon transport. In tectonically relaxed areas, hydraulically induced fractures propagate in the vertically and perpendicular to the minimum horizontal stress (MHS). Furthermore, the required fracture initiation and propagation pressures depend on the magnitude of the least principal stress (Hubbert and Willis, 1972).

I estimated the MHS gradient in Wells 1 and 2 using well logs and cross-validated the output with the available fracture closure pressure measurements obtained from multi-stage hydraulic fracture data from Well 2. Track 14 of **Figure 3**, and track 12 of **Figure 4**, illustrate the estimated MHS gradient in Wells 1 and 2, respectively. Track 15 of **Figure 3** and Track 14 of **Figure 4** show the results of geomechanical rock classification based on stress-profiles (SPRC), including high- (SPRC1), medium- (SPRC2), and low-MHS (SPRC3) levels. The results indicate that the MHS gradient varies considerably when moving across geologic facies. The MHS gradient ranges from 0.35-0.85 psi/ft (8-19 kPa/m), with the average MHS gradient of 0.58 psi/ft (13 kPa/m) in Well 1, and 0.62 psi/ft (14 kPa/m) in Well 2 in the lower Eagle Ford formation. **Table 6** summarizes the class-by-class statistics of the MHS gradient in both wells.

Rock class	Minimum Horizontal Stress Gradient	psi/ft (kPa/m)
	Well 1	**Well 2**
SPRC1	0.73 (16.5)	0.71 (16.1)
SPRC2	0.62 (14.0)	0.62 (14.0)
SPRC3	0.48 (10.9)	0.55 (12.4)

Table 6. Class-by-class statistics of the MHS gradient in Wells 1 and 2

The results of the classification based on MHS indicate a higher proportions of the low-stress rock class (i.e., SPRC3) in Well 1 (55% of gross thickness) compared to Well 2 (34% of gross thickness). **Figure 21** shows the histogram comparison of MHS gradient in the LEF for Well 1 and Well 2. The green bars represent SPRC3 where the MHS gradient is lower than 0.55 psi/ft (12.4 kPa/ft). Since fracture initiation and propagation in SPRC3 requires lower pressures, it is considered to be a better completion quality class compared to SPRC2 and SPRC1.

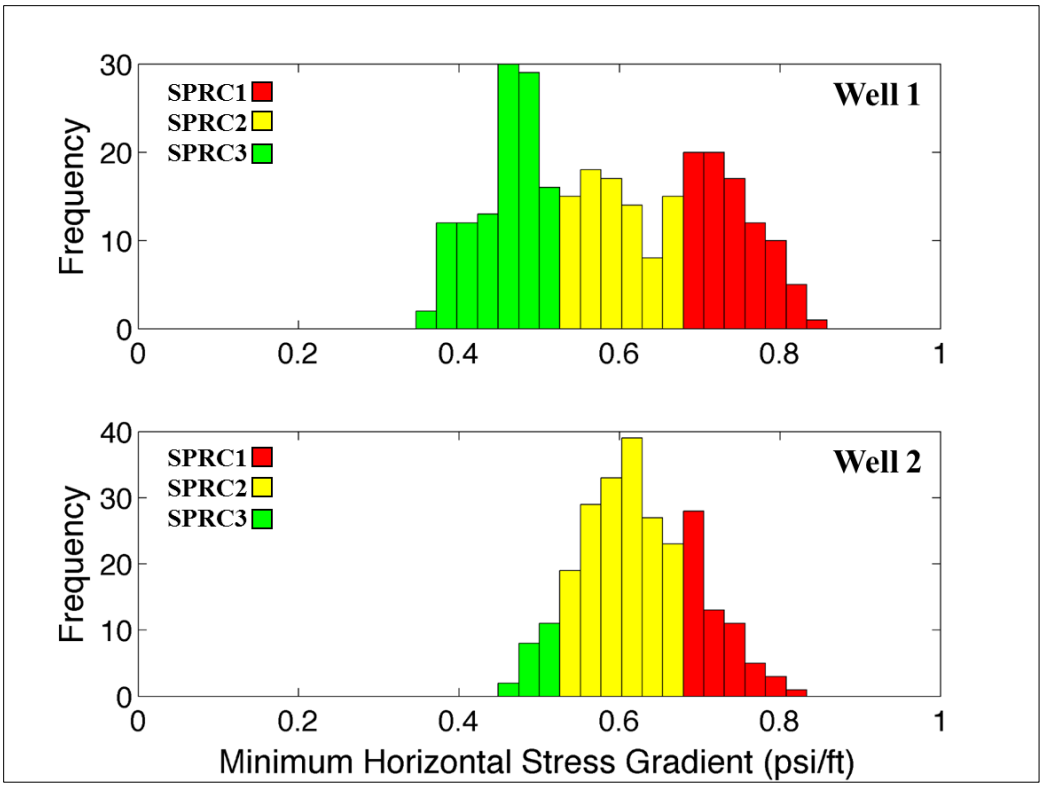

Figure 21. Histogram comparison of the MHS gradient in Well 1 and Well 2 in the lower Eagle Ford. Different colors represent different rock classes based on stress profiles.

3.7 Integrated Completion-Based Recommendation

Final recommendation of the best target interval for horizontal well placement and multi-stage hydraulic fracturing is based on an integration of the rock classifications in the pilot section of Wells 1 and 2. In this selection, I accounted for properties such as organic-richness, storage capacity, fluid saturations, volumetric concentrations of clay, and the minimum horizontal stress. Additionally, in Well 1, I included geological and geochemical characteristics of the selected target interval for decision making.

In Well 1, I selected XX430-XX470 ft as the best target interval for completions. Geologically, this interval represents the foraminiferal wackestone facies where the organic content can be as great as 6 wt%. Furthermore, the geochemical classification results indicated significant enrichment of trace elements such as vanadium and nickel, which correlated with higher hydrocarbon contents. Based on the petrophysical rock classification, this target interval contains the best reservoir quality class (PRC5) combined with PRC1, which represent the thinly-bedded limestone units. However, due to their low thickness, these limestone beds are not expected to act as barriers to the induced hydraulic fractures. Geomechanically, the selected target zone is a low-MHS rock, which makes it a good candidate for fracture initiation and propagation. A 5,000 ft (1,500 m) horizontal lateral at XX450 ft was landed in Well 1. Production history shows a 90-day production of 54,000 BOE.

For Well 2, I selected XX925-XX950 ft as the best target interval for completions. This target is a low-MHS interval adjacent to PRC5 rocks, which represent the best petrophysical rock class. In both wells, the upper part of the LEF appears to be ductile, with MHS estimates of greater than 0.75 psi/ft (15.8 kPa/m). A horizontal lateral with length of over 6,000 ft (1,800 m) was drilled and hydraulically fractured in Well 2. In most stages the fracture closure pressure gradient of 0.68 psi/ft (15.4 kPa/m) was observed. It is possible that the upper 30 ft (9 m) of the LEF in both wells act as a fracture barrier and contain the upward growth to the UEF formation. Production from

Well 2 for the first 90-days was 43,000 BOE, which is approximately 25% less than Well 1.

3.8 Comparison of Well Productivity

Figure 22 illustrates the cumulative 90-day hydrocarbon, and water production for Well 1 and Well 2. Well 1 produced a cumulative volume of 54,000 BOE hydrocarbons and 1,000 barrels (BBL) of water in the first 90 days after completions. Well 2 produced 43,000 BOE hydrocarbons and 10,000 BBL of water during the same time interval.

For Wells 1 Well 2, I observed nearly similar petrophysical properties including organic-richness, storage capacity, fluid saturations, and total volumetric concentration of clay in the reservoir quality rock classes. However, the geomechanical analysis showed a different distribution of stress profiles between these wells. Overall, Well 1 contains higher proportions and a better vertical continuity of low-MHS rock units, as well as a slightly lower average MHS in the LEF, compared to Well 2. Furthermore, I observed thinly-bedded limestone intervals in Well 1 and thicker limestone layers in Well 2, which may act as barriers to hydraulic fracture growth. This difference in stratigraphic distribution of rock classes and MHS can impact the vertical propagation of hydraulically induced fractures, and consequently the total stimulated reservoir volume. Although the presence of natural fractures was not investigated due to unavailability of

image logs, the different geomechanical characteristics between these wells can potentially explain the well production difference.

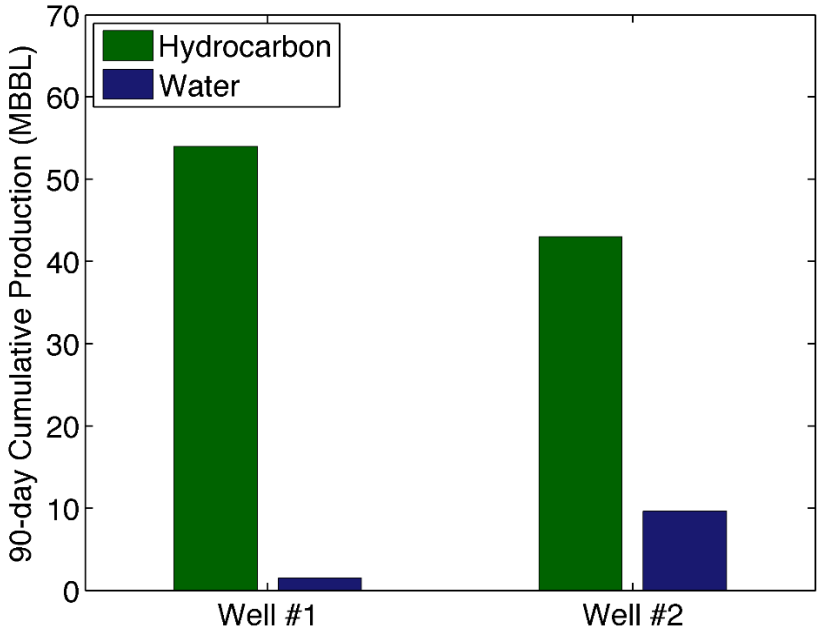

Figure 22. Cumulative 90-day hydrocarbon and water production from Well 1 and Well 2. Green and blue bars represent hydrocarbon and water production, respectively.

4. CONCLUSIONS

4.1 Summary

The objective of this thesis was to introduce an integrated well-log-based rock classification method that takes into account geological, geochemical, petrophysical, and geomechanical properties of the formation. The results included the application of this method to the pilot section of two wells located approximately 20 miles apart, just north of the Edwards Shelf Margin, in the oil window of the Eagle Ford Shale play. I initially used Well 1 to build and validate a well-log-based petrophysical rock classification model with core-based geological and geochecmical rock classifications. Lithofacies descriptions were generated based on the analysis of rock texture, using core and thin-section images. Further, I analyzed the elemental distribution throughout the formation, and identified unique chemostratigraphic units based on the XRF-derived elemental concentrations from the core samples. Finally, I conducted a geomechanical rock classification based on the minimum horizontal stress gradients in the LEF, and recommended target intervals for well completions (horizontal well placement and multi-stage hydraulic fracturing) based on an integrated analysis of the four aforementioned rock classification results. The main contributions of this research compared to the previously introduced rock classification techniques are:

- Integration of core-based geologic and geochemical data with well-log-based petrophysical rock classification.

- Incorporation of a well-log-based geomechanical properties (i.e., in-situ stress profile), based on in-situ stress profiles, into the petrophysical rock classification scheme for recommendation of completion intervals and comparison of well productivity among different wells.

4.2 Conclusions

Results of this thesis indicates that the best reservoir quality rocks (PRC5) in the LEF are associated with bedded foraminiferal wackestone facies, where the TOC averages at 5 wt%, with porosity of 7% and total volumetric concentration of clays between 10-15%. The concentration of certain trace elements such as Ni and V in the LEF (from core XRF measurements) correlate directly with in-situ hydrocarbon content obtained from Rock-Eval measurements (V appears to correlate better with the S1, compared to Ni). The organic-rich foraminiferal wackestone facies are stratigraphically located in the upper part of LEF, and are considered as the main targets for horizontal lateral placement in the wells included in this research. Furthermore, it is apparent that the reservoir quality is significantly reduced in the bottom interval of LEF, where kaolinitic clays make up greater proportions of the rock volume (i.e., up to 14 vol%). Despite of a moderate TOC (i.e., 2-3 wt%), these mudstones lack storage capacity with porosity values of lower than 4%.

The production comparison between Wells 1 and 2, which are petrophysically similar suggests the importance of geomechanical properties in the assessment of well

productivity. Well 1, with higher proportions of low-MHS (completion quality) rock class produced an excess of 11,000 BOE (i.e., 25 vol%, relative to Well 2) in the first 90 days after fracture stimulation. The results demonstrated that the well-by-well difference in production cannot be explained by only relying on the estimated petrophysical properties of the formation. In addition, the geomechanical properties such as in-situ stresses and presence of natural fractures (which was not studied in this research due to data limitations) play important roles towards well productivity and must be taken into account in rock classification for completion decisions. Finally, to be able to strengthen the conclusions derived in this research, application of the well-log-based rock classification to more wells located in the area of interest is recommended.

REFERENCES

Archie, G. E., 1952, Classification of Carbonate Reservoir Rocks and Petrophysical Considerations, *AAPG Bulletin*, **36**(2), 278-298.

Aderibigbe, A., Chen Valdes, C., and Heidari, Z., 2016, Integrated Rock Classification in the Wolfcamp Shale Based on Reservoir Quality and Anisotropic Stress Profile Estimated from Well Logs, *Interpretation*, **4**(2), SF1-SF18.

Bardon, C. and Pied, B., 1969, Formation Water Saturation in Shaly Sands, Paper SPWLA-1969-Z presented at SPWLA 10th Annual Logging Symposium, Houston, Texas, USA, 25-28 May.

Berryman, J.G., 1995, Mixture Theories for Rock Properties, *Rock Physics & Phase Relations: A Handbook of Physical Constants*, 205-228.

Brumsack, H. J., 2006, The Trace Metal Content of Recent Organic Carbon-rich Sediments: Implications for Cretaceous Black Shale Formation, *Palaeogeography, Palaeoclimatology, Palaeoecology*, **232**(2), 344-361.

Dawson, W. C., 2000, Shale Microfacies: Eagle Ford Group (Cenomanian-Turonian) North-central Texas Outcrops and Subsurface Equivalents, *Gulf Coast Association of Geological Societies Transactions*, **50**, 607-621.

Donovan, A.D. and Staerker, T.S., 2010, Sequence Stratigraphy of the Eagle Ford (Boquillas) Formation in the Subsurface of South Texas and Outcrops of West

Texas, *Gulf Coast Association of Geological Societies Transactions*, **60**, 861-899.

Driskill, B., Suurmeyer, N., Rilling-Hall, S., Govert, A. M., and Garbowicz, A., 2012, Reservoir Description of the Subsurface Eagle Ford Formation, Maverick Basin Area, South Texas, USA, Paper SPE-154528-MS presented at SPE Europec/EAGE Annual Conference, Copenhagen, Denmark, 4-7 June.

Dunham, R. J., 1962, Classification of Carbonate Rocks According to Depositional Textures, In: Ham, W.E., Ed., Classification of Carbonate Rocks, *American Association of Petroleum Geologists*, 108-121.

Fairbanks, M. D., 2012, *High Resolution Stratigraphy and Facies Architecture of the Upper Cretaceous (Cenomanian-Turonian) Eagle Ford group, Central Texas*, M.Sc. Thesis, University of Texas, Austin.

Faust, M.J., 1990, Seismic Stratigraphy of the mid-Cretaceous Unconformity (MCU) in the Central Gulf of Mexico Basin, *Geophysics*, **55**(7), 868-884.

Folk, R. L., 1962, Spectral Subdivision of Limestone Types, in Ham, W.E., Ed., Classification of Carbonate Rocks – A Symposium, *American Association of Petroleum Geologists Memoir* **1**, 62-84.

Grabau, A.W., 1904, On the Classification of Sedimentary Rocks, *American Geologist*, Place of Publication not Identified.

Harbor, R. L., 2011, Facies Characterization and Stratigraphic Architecture of Organic-rich Mudrocks, Upper Cretaceous Eagle Ford Formation, South Texas, M.Sc. Thesis, University of Texas, Austin.

Hentz, T. F., and Ruppel, S. C., 2010, Regional Lithostratigraphy of the Eagle Ford Shale: Maverick Basin to East Texas Basin, *Gulf Coast Association of Geological Societies Transactions*, **60**, 325-337.

Hubbert, M.K., and David G. Willis, 1972, Mechanics of Hydraulic Fracturing, *American Association of Petroleum Geologists Memoir* **18**, 239-257.

Kale, S., Rai, C. and Sondergeld, C., 2010, Rock Typing in Gas Shales, Paper SPE-134539-MS presented at SPE Annual Technical Conference and Exhibition, Florence, Italy, 19-22 September.

Lewan, M.D., 1984, Factors Controlling the Proportionality of Vanadium to Nickel in Crude Oils, *Geochimica et Cosmochimica Acta*, **48**(11), 2231-2238.

Lock, B. E., Peschier, L., and Whitcomb, N., 2010, The Eagle Ford (Boquillas Formation) of Val Verde County, Texas-A Window on the South Texas Play, *Gulf Coast Association of Geological Societies Transactions*, **60**, 419-434.

Lowery, C.M., Corbett, M.J., Leckie, R.M., Watkins, D., Romero, A.M. and Pramudito, A., 2014, Foraminiferal and Nannofossil Paleoecology and Paleoceanography of the Cenomanian–Turonian Eagle Ford Shale of Southern Texas, *Palaeogeography, Palaeoclimatology, Palaeoecology*, **413**, 49-65.

Mavko, G., Mukerji, T. and Dvorkin, J., 2009, The Rock Physics Handbook: Tools for Seismic Analysis of Porous Media, *Cambridge University Press*.

Petriello, J., Marino, S., Suarez-Rivera, R., Handwerger, D. A., Herring, S., Woodruff, W., and Stevens, K., 2013, Integration of Quantitative Rock Classification with Core-Based Geologic Studies: Improved Regional-Scale Modeling and Efficient Exploration of Tight Shale Plays, Paper 167048-MS presented at SPE Unconventional Resources Conference and Exhibition-Asia Pacific, Brisbane, Australia , 11-13 November.

Popielski, A. C., Heidari, Z., and Torres-Verdin, C., 2012, Rock Classification from Conventional Well Logs in Hydrocarbon-Bearing Shale, Paper 159255-MS presented at SPE Annual Technical Conference and Exhibition, San Antonio, Texas, USA, 8-10 October.

Prasad, M., Kopycinska, M., Rabe, U., and Arnold, W., 2002, Measurement of Young's Modulus of Clay Minerals using Atomic Force Acoustic Microscopy. *Geophysical Research Letters*, **29**(8), 13-1–13-4.

Quirein, J., Witkowsky, J., Truax, J. A., Galford, J. E., Spain, D. R., and Odumosu, T., 2010, Integrating Core Data and Wireline Geochemical Data for Formation Evaluation and Characterization of Shale-Gas Reservoirs, Paper 134559-MS presented at SPE Annual Technical Conference and Exhibition, Florence, Italy, 19-22 September.

Rushing, J. A., Newsham, K. E., and Blasingame, T. A., 2008, Rock Typing: Keys to Understanding Productivity in Tight Gas Sands. Paper 114164-MS presented at SPE Unconventional Reservoirs Conference, Keystone, Colorado, USA, 10-12 February.

Saneifar, M., A. Aranibar, and Z. Heidari, 2014, Rock Classification in the Haynesville Shale based on Petrophysical and Elastic Properties Estimated from Well Logs: *Interpretation*, **3**(1), SA65–SA75.

Sone, H. and Zoback, M.D., 2013, Mechanical Properties of Shale-gas Reservoir Rocks—Part 1: Static and Dynamic Elastic Properties and Anisotropy, *Geophysics*, **78**(5), D381-D392.

Suarez-Rivera, R., Deenadayalu, C., Chertov, M., Hartanto, R.N., Gathogo, P. and Kunjir, R., 2011, Improving Horizontal Completions on Heterogeneous Tight-Shales, Paper SPE-146998-MS presented at Canadian Unconventional Resources Conference, Calgary, Alberta, Canada, 15-17 November.

Tian, Y., Ayers, W.B. and McCain Jr, D., 2013, March. The Eagle Ford Shale play, South Texas: Regional Variations in Fluid Types, Hydrocarbon Production and Reservoir Properties, Paper IPTC-16808-MS presented at International Petroleum Technology Conference, Beijing, China, 26-28 March.

Tian, Y., Ayers, W. B., and McCain, W. D., 2014, Regional Impacts of Lithologic Cyclicity and Reservoir and Fluid Properties on Eagle Ford Shale Well

Performance, Paper SPE-169007-MS presented at Society of Petroleum Engineers, Woodlands, Texas, 1-3 April.

Tribovillard, N., Algeo, T. J., Lyons, T., and Riboulleau, A., 2006, Trace Metals as Paleoredox and Paleoproductivity Proxies: An Update, *Chemical geology*, **232**(1), 12-32.

Vanorio, T., Prasad, M., and Nur, A., 2003, Elastic Properties of Dry Clay Mineral Aggregates, Suspensions and Sandstones, *Geophysical Journal International*, **155**(1), 319-326.

Ward Jr, J. H., 1963, Hierarchical Grouping to Optimize an Objective Function. *Journal of the American Statistical Association*, **58**(301), 236-244.

Wehner, M., Tice, M. M., Pope, M. C., Gardner, R., Donovan, A. D., and Staerker, T. S., 2015, Anoxic, Storm Dominated Inner Carbonate Ramp Deposition of Lower Eagle Ford Formation, West Texas, Paper URTEC-2154667-MS presented at Unconventional Resources Technology Conference, San Antonio, Texas, USA, 20-22 July.

Wilde, P., Lyons, T. W., and Quinby-Hunt, M. S., 2004, Organic Carbon Proxies in Black Shales: Molybdenum, *Chemical Geology*, **206**(3), 167-176.

Workman, S. J., 2013, *Integrating Depositional Facies and Sequence Stratigraphy in Characterizing Unconventional Reservoirs: Eagle Ford Shale, South Texas*, M.Sc. Thesis, Western Michigan University, Kalamazoo, Michigan.

Wright, A. M., and Ratcliffe, K., 2010, Application of Inorganic Whole Rock Geochemistry to Shale Resource Plays, Paper SPE-137946-MS presented at Canadian Unconventional Resources and International Petroleum Conference, Calgary, Alberta, Canada, 19-21 October.